12-2023

Subduction Initiation Recorded in the Dadeville Complex of Alabama and Georgia, Southeastern United States

Naomi A. Becker
Johns Hopkins University

Freya R. George
Johns Hopkins University

George L. Guice
Johns Hopkins University

James L. Crowley
Boise State University

Wendy R. Nelson
Towson University

See next page for additional authors

Research Paper

GEOSPHERE

GEOSPHERE, v. 19, no. 6

https://doi.org/10.1130/GES02643.1

9 figures; 2 tables; 1 set of supplemental files

CORRESPONDENCE: nbecker@jhu.edu, naomiannbecker@gmail.com

CITATION: Becker, N.A., George, F.R., Guice, G.L., Crowley, J.L., Nelson, W.R., Browning-Hanson, J.F., Roy, S., and Viete, D.R., 2023, Subduction initiation recorded in the Dadeville Complex of Alabama and Georgia, southeastern United States: Geosphere, v. 19, no. 6, p. 1729–1746, https://doi.org/10.1130/GES02643.1.

Science Editor: Andrea Hampel
Associate Editor: Wentao Cao

Received 30 January 2023
Revision received 11 August 2023
Accepted 28 August 2023

Published online 27 October 2023

GOLD OPEN ACCESS

THE GEOLOGICAL SOCIETY OF AMERICA®

Subduction initiation recorded in the Dadeville Complex of Alabama and Georgia, southeastern United States

Naomi A. Becker[1], Freya R. George[1,2], George L. Guice[1,3,4], James L. Crowley[5], Wendy R. Nelson[4], Joseph F. Browning-Hanson[1], Supratik Roy[1], and Daniel R. Viete[1]

[1]Department of Earth & Planetary Sciences, Johns Hopkins University, 3400 N. Charles Street, Baltimore, Maryland 21218, USA
[2]School of Earth Sciences, University of Bristol, Wills Memorial Building, Bristol, BS8 1RJ, UK
[3]Department of Earth and Planetary Sciences, American Museum of Natural History, New York, New York 10024, USA
[4]Department of Physics, Astronomy and Geosciences, Towson University, 8000 York Road, Towson, Maryland 21252, USA
[5]Department of Geosciences, Boise State University, 1910 W University Drive, Boise, Idaho 83725, USA

ABSTRACT

The Dadeville Complex of Alabama and Georgia (southeastern United States) represents the largest suite of exposed mafic-ultramafic rocks in the southern Appalachians. Due to poor preservation, chemical alteration, and tectonic reworking, a specific tectonic origin for the Dadeville Complex has been difficult to deduce. We obtained new whole-rock and mineral geochemistry coupled with zircon U-Pb geochronology to investigate the magmatic and metamorphic processes recorded by the Dadeville Complex, as well as the timing of these processes. Our data reveal an up-stratigraphic evolution in the geochemistry of the volcanic rocks, from forearc basalts to boninites. Our new U-Pb zircon crystallization data—obtained from three amphibolite samples—place the timing of forearc/protoarc volcanism no later than ca. 467 Ma. New thermobarometry suggests that the Dadeville Complex rocks subsequently experienced deep, high-grade metamorphism, at pressure-temperature conditions of >7 kbar and >760 °C. The data presented here support a model for formation of the Dadeville Complex in the forearc region of a subduction zone during subduction initiation and protoarc development, followed by deep burial/underthrusting of the complex during orogenesis.

1. INTRODUCTION

The Appalachian-Caledonian orogen formed in response to the closure of the Iapetus and Rheic Oceans and subsequent continental collisions producing the supercontinent Pangea. During convergence, sections of oceanic lithosphere were emplaced onto the continents and preserved along the >6500 km (from current-day southeastern United States to northern Norway and Sweden) Iapetan margin (Bird et al., 1971; Bird and Dewey, 1970; Hibbard et al., 2007; Pedersen and Furnes, 1991; Pedersen et al., 1988; Waldron et al., 1996). The oceanic record is more robust in the northern Appalachians and Caledonides, where well-exposed ophiolites (obducted oceanic crust) with near-complete lithospheric sections (e.g., the Bay of Islands and Betts Cove ophiolites, Canada, and the Solund-Stavfjord ophiolite, Norway) preserve a record of subduction zone processes in the Iapetus Ocean (Bédard, 1999; De Souza et al., 2008; Furnes et al., 1988; Olive et al., 1997; Oliver and McAlpine, 1998). In contrast, the southern Appalachians have a paucity of complete ophiolites, with oceanic rocks instead forming smaller complexes of mafic and ultramafic rocks (Crowley, 1976; Drake and Morgan, 1981; Guice et al., 2021; McElhaney and McSween, 1983; Misra and Conte, 1991; Mittwede, 1989; Tenthorey et al., 1996; Raymond et al., 2003, 2016; Peterson and Ryan, 2009; Spell and Norrell, 1990). The differences between the northern and southern sections of the Appalachian-Caledonian orogen have long been recognized, and studies have sought to correlate major events in the orogen's history using ophiolites and mafic-ultramafic complexes as markers for suture zones between terranes and continents (Hibbard et al., 2007, and references therein). For these correlations to be effectively made, the specific tectonic formation settings of the southern Appalachian mafic-ultramafic complexes must first be determined.

Studies of a modern subduction zone—the Izu-Bonin-Mariana system—have resulted in a model for correlating magmatic products with their associated tectonic setting within the subduction system (Arculus et al., 2015; Barth and Gluhak, 2009; Dilek and Thy, 2009; Ishizuka et al., 2011; Ishikawa et al., 2002; Leng et al., 2012; Li et al., 2021; Pearce et al., 2015; Pearce and Reagan, 2019; Portnyagin et al., 1997; Reagan et al., 2010, 2019; Rioux et al., 2021; Shervais et al., 2004, 2019, 2021; Stern et al., 2012; Whattam and Stern, 2011; Yuan et al., 2005). In the Izu-Bonin-Mariana model, forearc basalts—formed from decompression melting of the mantle during subduction-triggered extension—are the first to erupt, forming the base of the forearc volcanic stratigraphy (Reagan et al., 2010; Pearce and Reagan, 2019), whereas boninites—formed from subsequent flux melting of the depleted mantle as the volcanic arc system is established—overlie the forearc basalts (Ishizuka et al., 2011; Reagan et al., 2019; Shervais et al., 2019, 2021). On the basis

Naomi Becker https://orcid.org/0000-0003-0102-9713

of geochemistry, suprasubduction zone ophiolites have been interpreted as representing the backarc, arc, and/or forearc regions of a subduction zone, or as capturing some combination of these settings within an evolving system (Dilek and Furnes, 2011, and references therein). Of these settings, the forearc lithosphere is the most widely recorded in Phanerozoic ophiolites (Stern et al., 2012), with recognition of this tectonic setting based on a distinctive up-stratigraphic record of volcanic evolution from forearc basalts to boninites. The Izu-Bonin-Mariana model can be utilized to identify ophiolites and mafic-ultramafic complexes that record subduction initiation and forearc spreading throughout the Appalachian-Caledonian orogen, allowing for temporal correlation of subduction initiation processes over >6500 km.

This study considered samples from the Dadeville Complex of Alabama and Georgia, the southernmost exposed sequence of mafic-ultramafic rocks in the Appalachian orogen. Whole-rock and mineral geochemical analyses coupled with U-Pb zircon geochronology were utilized to investigate the origin of the Dadeville Complex and to place it more clearly within the context of Appalachian tectonic history.

2. GEOLOGIC BACKGROUND

2.1. Appalachian Orogen

The southern Appalachian orogen can be subdivided into three domains based on differing tectonic origins: (1) the Laurentian realm, (2) the Iapetan realm, and (3) the peri-Gondwanan realm (Hibbard et al., 2007). The Laurentian realm (Rankin, 1994) encompasses the foreland and western Blue Ridge/Talladega terrane (Fig. 1A), which is composed of rocks formed on or adjacent to Laurentia that record the Grenville orogeny and the rift-to-drift sequences deposited during the breakup of eastern Rodinia (Hibbard et al., 2007). The Iapetan realm predominantly contains rocks that formed within the Iapetus Ocean—including oceanic lithosphere and island arcs. The Iapetan realm is separated into the Dunnage zone north of the New

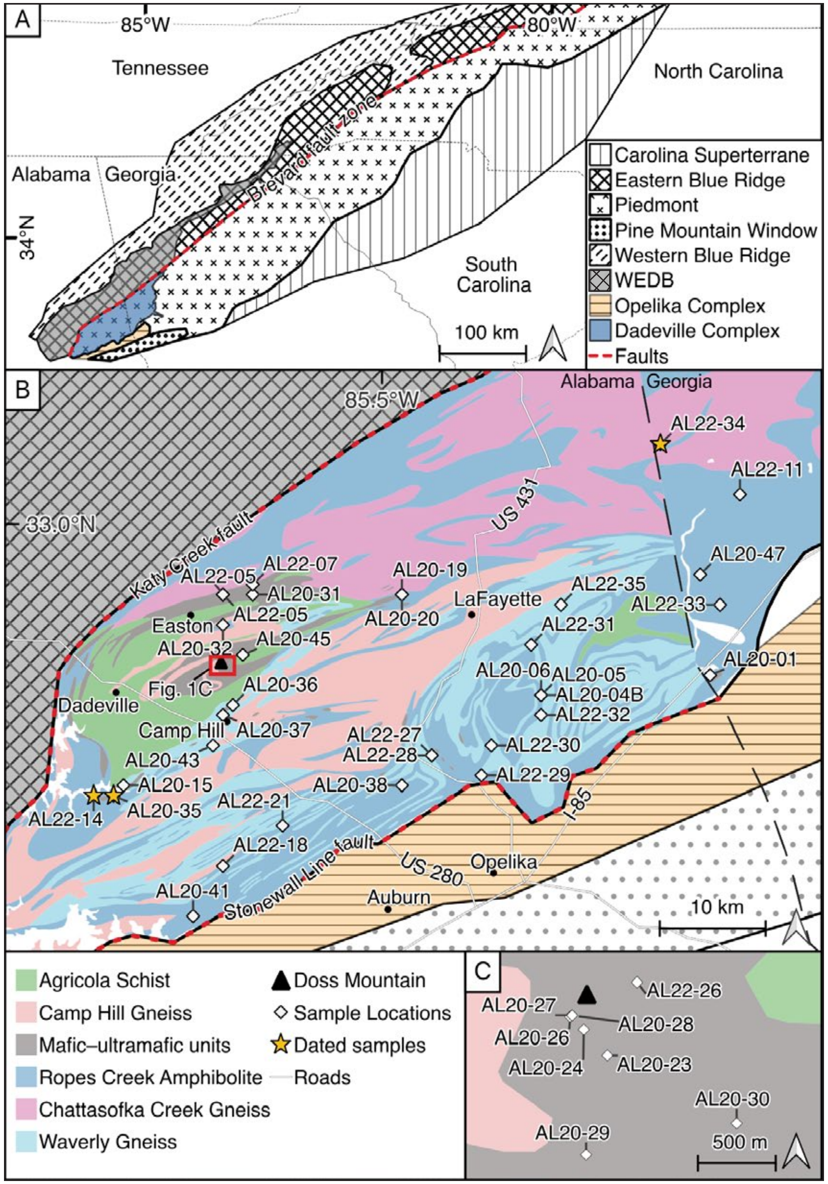

Figure 1. (A) Geologic map of the southern Appalachian orogen (modified from Pollock et al., 2012) showing major terrane divisions and locations of the Dadeville and Opelika Complexes. (B) Geologic map of the Dadeville Complex of Alabama and Georgia (modified from Tull et al., 2014) showing lithologic units and locations of petrological/geochemical samples for this study (stars indicate samples also dated by U-Pb zircon geochronology). (C) Sample locations in Doss Mountain area. WEDB—Wedowee-Emuckfaw-Dahlonega basin.

York embayment (the narrowest exposed portion of the orogen) and the Piedmont domain to the south (Hibbard et al., 2007). The peri-Gondwanan realm consists of Gondwana-derived terranes that were accreted to the Laurentian margin during the closure of the Iapetus and Rheic Oceans (Adams et al., 1995; Horton et al., 1989; Miller et al., 2006; Muller et al., 1989; Stewart et al., 1997). Notable peri-Gondwanan terranes include Ganderia, Avalonia, and Meguma in the northern Appalachians and the Carolina superterrane and Suwannee terrane in the southern Appalachians (Hibbard et al., 2007; Pollock et al., 2012; Rodgers, 1971; Williams and Hatcher, 1983).

2.2. Piedmont Domain

The Piedmont domain of the southern Appalachians includes the Inner Piedmont and the eastern Blue Ridge terranes, which predominantly consist of metamorphosed clastic lithologies with rare magmatic arc and oceanic rocks (Coler et al., 2000; Hibbard et al., 2007; Horton et al., 1998; Seal and Kish, 1990). The Brevard fault zone (Fig. 1A) separates the Piedmont domain from the eastern Blue Ridge terrane (Hibbard et al., 2007; Spell and Norrell, 1990). The Inner Piedmont is a composite terrane that contains oceanic and magmatic arc rocks with depleted incompatible element and enriched fluid-mobile element signatures interpreted to suggest a subduction zone origin (Coler et al., 2000; Hibbard et al., 2007; Horton et al., 1998; Merschat et al., 2018; Seal and Kish, 1990). The eastern Blue Ridge is predominantly composed of deep-water sedimentary units; however, several interlayered metasedimentary and mafic/bimodal volcanic suites have collectively been interpreted to represent a ca. 470–430 Ma backarc basin, the Wedowee-Emuckfaw-Dahlonega basin, which extends from Alabama to North Carolina (Barineau et al., 2015; Tull et al., 2014). The Opelika Complex—located southeast of the Dadeville Complex—was originally assigned to the Inner Piedmont but has since been correlated with units to the northwest of the Dadeville Complex and reclassified as part of the eastern Blue Ridge (Stevens, 2018).

2.3. Dadeville Complex

The Dadeville Complex is situated within the Inner Piedmont at the southernmost exposed end of the Appalachians (Fig. 1A). It consists of felsic and mafic metavolcanic rocks, felsic and mafic-ultramafic intrusions, and metasedimentary units (Fig. 1B; Steltenpohl et al., 2013; Tull et al., 2018). Bordered to the northwest by the Katy Creek fault (part of the Brevard fault zone) and to the southeast by the Stonewall Line fault (Tull et al., 2018; Vandervoort, 2016), the Dadeville Complex has been interpreted as a klippe within the Tallahassee synform, structurally overlying the Wedowee-Emuckfaw-Dahlonega basin units to the northwest and the Opelika Complex to the southeast (Stevens, 2018; Tull et al., 2018).

The basal unit of the Dadeville Complex is the Ropes Creek Amphibolite, which accounts for roughly 40% of the exposed outcrop (Tull et al., 2018). The Ropes Creek Amphibolite is a layered, basaltic amphibolite with subordinate amounts of intercalated dacitic volcanics and metasedimentary units (Tull et al., 2018), and it is interpreted as metamorphosed basalt flows formed in an extensional oceanic setting (Stow et al., 1984). Zircon Hf isotope values from an intercalated dacite layer in the Ropes Creek Amphibolite suggest involvement of a depleted mantle source during formation (Tull et al., 2018). The Ropes Creek Amphibolite occurs in close association with two other units of the Dadeville Complex, the Waresville Formation—recently interpreted as synonymous with the Ropes Creek Amphibolite (Farris et al., 2017)—and the andesitic-dacitic Waverly Gneiss, which is intercalated with the Ropes Creek Amphibolite in the eastern portion of the complex (Ma et al., 2019). The Ropes Creek Amphibolite and Waverly Gneiss units are named and mapped separately on the *Geologic Map of Alabama* (Osborne et al., 1989), but on the *Geologic Map of Georgia*, they are undifferentiated and collectively mapped as "hornblende gneiss/amphibolite" (Lawton et al., 1976).

Other major units of the Dadeville Complex include the Agricola Schist, the Camp Hill Gneiss, the Chattasofka Creek Gneiss (Rock Mills Gneiss or Franklin Gneiss in Georgia), and various small occurrences of mafic-ultramafic rocks. The uppermost unit—the Agricola Schist—is a pelitic to psammitic schist that records metamorphic conditions of 5–8 kbar and 600–700 °C (Drummond et al., 1997; Tull et al., 2018), and its sedimentary deposition has been linked to either an intra-arc basin or a cover sequence (Ma et al., 2019; Tull et al., 2018). The Camp Hill Gneiss—intrusive to the Ropes Creek Amphibolite and the Agricola Schist—is a trondhjemite-tonalite pluton that is interpreted as the product of partial melting of a basaltic protolith under middle- to upper-crustal pressures (Drummond et al., 1997; Neilson et al., 1997; Sterling, 2006). The Chattasofka Creek Gneiss—intrusive to the Ropes Creek Amphibolite, the Agricola Schist, and the Doss Mountain suite—is considered to be a syncollisional granite originating from a metapelitic protolith (Davis, 2021; Drummond et al., 1997; Nielson et al., 1997; Sterling, 2006). Rocks interpreted as mafic-ultramafic intrusions into the Ropes Creek Amphibolite occur as small bodies throughout the complex (Davis, 2021; Drummond et al., 1997; Nielson et al., 1997; Sterling, 2006). The largest of these mafic-ultramafic units, the Doss Mountain suite, is comprised of pyroxenite and gabbronorite lithologies (Davis, 2021; Farris et al., 2017; Neilson, 1983; Neilson and Bittner, 1990; Neilson and Stow, 1986).

Previous zircon U-Pb geochronology on Dadeville Complex units performed by laser ablation–inductively coupled plasma–mass spectrometry (LA-ICP-MS) yielded crystallization dates of ca. 458 Ma, ca. 430 Ma, and ca. 465 Ma for the Ropes Creek Amphibolite/Waresville Formation, ca. 454 Ma for the Waverly Gneiss, ca. 480 Ma and ca. 448–446 Ma for the Camp Hill Gneiss, ca. 449 Ma for the Chattasofka Creek Gneiss, and ca. 394 Ma for a felsite within the Agricola Schist (Ma et al., 2019; Tull et al., 2018). Overgrowths on zircons from the Waverly Gneiss samples yielded a date of ca. 402 Ma, interpreted as the timing of peak metamorphism (Ma et al., 2019). Detrital zircon populations from the Agricola Schist and other metasedimentary units near the base of the Ropes Creek Amphibolite as well as felsic layers within other units showed a strong Grenvillian signature, indicating formation on or close to the Laurentian margin (Tull et al., 2018). Negative εNd values from the Doss Mountain suite and other mafic-ultramafic rocks suggest extraction from an evolved source and/or interaction with continental lithosphere (Tull et al., 2018).

Geochemical studies of the Doss Mountain suite, Camp Hill Gneiss, and Chattasofka Creek Gneiss indicated whole-rock major- and trace-element compositions that exhibit volcanic arc signatures (Neilson et al., 1997; Stow et al., 1984). When coupled with the similarly aged Wedowee-Emuckfaw-Dahlonega basin to its northwest, the Dadeville Complex has been hypothesized to represent the arc component of a paired arc-backarc system (Barineau et al., 2015; Tull et al., 2014). Taken with existing geochronology, the current interpretation is that the Dadeville Complex represents a dismembered volcanic arc that was accreted (with its conjugate backarc, the Wedowee-Emuckfaw-Dahlonega basin) onto Laurentia during Appalachian continental collision (Farris et al., 2017; Ma et al., 2019).

3. SAMPLES AND FIELD RELATIONSHIPS

Forty-one samples were collected from the Dadeville Complex. Twenty-eight samples were collected from within the mapped regions of the Ropes Creek Amphibolite, the Waverly Gneiss, or unnamed mafic-ultramafic rocks (Fig. 1B; Neilson et al., 1997; Neilson and Stow, 1986; Stow et al., 1984). Ten samples were collected in situ from the Doss Mountain suite (Fig. 1C; Neilson and Stow, 1986), and two additional samples were collected as float. One sample was collected from the Easton Complex of Neilson and Stow (1986). The majority of the Dadeville Complex is heavily weathered, with fine- to medium-grained mafic units primarily consisting of saprolite with preserved corestones. The medium-grained Doss Mountain suite and mafic-ultramafic rocks are better preserved than the Ropes Creek Amphibolite and associated units. For additional descriptions of lithologic units and field relationships, see Neilson and Bittner (1990) and Farris et al. (2017).

4. ANALYTICAL METHODS

Full details of the methods for bulk-rock geochemistry and geochronology are available in Supplemental Material Item B[1], with summaries presented here.

4.1. Bulk-Rock Geochemistry

All samples had weathered materials removed and were crushed and powdered. A split of powder from each sample was sent to the Franklin and Marshall X-Ray Laboratory, where 0.4 g of powder was flux melted in the presence of lithium tetraborate and then quenched to produce a glass disc. Major-element analysis was performed on the glass disc using a Malvern PANalytical, Inc., Zetium X-ray fluorescence (XRF) spectrometer. Shards of the glass discs used for XRF analyses were mounted in 1" (2.5 cm) epoxy rounds, polished, and then analyzed for trace elements by LA-ICP-MS using a Teledyne-Cetac Analyte G2 193 nm laser coupled to an Agilent 8900 quadrupole ICP-MS in the TeMPO Laboratory, Johns Hopkins University (JHU). Data were collected using 600 μm line scans with a pre-ablation pass to remove surface contamination. Analyses were conducted using a scan speed of 10 μm/s, laser repetition rate of 10 Hz, fluence of 4 J/cm^2, and an analytical mask that produced a square analysis spot with dimensions 50 × 50 μm. Integration time for each isotope was 0.1 s. Prior to each line scan, baseline measurements were made for 15 s. Standard reference glasses NIST 610, NIST 612, AGV-2G, BCR-2G, and/or BHVO-2G (Jochum et al., 2005) were measured after every seven unknown analyses. Data were processed using Iolite v4 (Paton et al., 2011), employing the trace-element reduction scheme and using ^{43}Ca (determined using XRF) as the internal standard. NIST 612 was used as the primary standard for data reduction, and data accuracy was assessed using the additional standards (NIST 610, AGV-2, BCR-2G, and/or BHVO-2G). Estimates of uncertainties for measurements of all elements are reported in Supplemental Material Item A.

4.2. Geochronology

4.2.1. Sample Preparation

Samples selected for zircon U-Pb analysis were crushed using a stainless-steel ring-and-puck mill, sieved to <500 μm, and washed to remove clay-sized particles. Washed samples were subjected to magnetic separation using a Frantz magnetic separator targeting isolation of a highly nonmagnetic fraction likely to be zircon enriched. The highly nonmagnetic fraction was then subjected to density separation using a sodium polytungstate (SPT) heavy liquid medium following the method of Andò (2020). Heavy mineral separates were inspected, and zircons were picked and then annealed in a muffle furnace at 900 °C for 60 h. The annealed zircons were mounted and polished by hand to expose grain cores for analysis.

4.2.2. Cathodoluminescence Imaging and LA-ICP-MS

Polished mounts were carbon coated and then imaged with cathodoluminescence (CL) using a Deben Centaurus CL detector mounted on a Thermo Scientific Helios G4 UC scanning electron microscope in the Materials Characterization and Processing Facility, JHU. Mounted and CL-imaged zircons were analyzed by the aforementioned LA-ICP-MS instrumentation in the TeMPO Laboratory. Each analysis followed 25 s of washout and comprised three cleaning shots and 250 analytical shots, using a laser repetition rate of 10 Hz, fluence of 2 J/cm^2, and a square aperture of 20 × 20 μm or 40 × 40 μm. The ^{204}Pb, ^{206}Pb, ^{207}Pb, ^{208}Pb, ^{232}Th, and ^{238}U isotopes were measured, repeating a 1 s

[1]Supplemental Material. Item A: Word file detailing the complete methods for mineral separation and chemical abrasion–isotope dilution–thermal ionization mass spectrometry (CA-ID-TIMS) analysis. Item B: Excel file containing all raw data presented in the manuscript. Please visit https://doi.org/10.1130/GEOS.S.24066384 to access the supplemental material, and contact editing@geosociety.org with any questions.

analytical cycle that used integration times of 0.1 s for the Th and U isotopes and 0.2 s for each of the Pb isotopes. Helium carrier gas flows were 0.38 L/min into cell and 0.35 L/min into the ablation cup, and Ar make-up gas was added to the analyte stream at a rate of 0.9 L/min prior to injection into the ICP-MS. "SQUID" tubing was used to smooth the signal at the detector. Standard reference zircons 91500 (1063.6 ± 0.3 Ma; Wiedenbeck et al., 1995; Schoene et al., 2006), Plešovice (337.13 ± 0.37 Ma; Sláma et al., 2008), Temora II (416.78 ± 0.33 Ma; Black et al., 2004), and FC-1 (1099.9 ± 1.1 Ma; Paces and Miller, 1993) were measured after every nine unknown analyses; the primary standard used for data reduction was 91500, with all others used to verify accuracy. Data reduction was performed in Iolite v4 (Paton et al., 2011) using a median fit to the standard data and including the U-Pb zircon geochronology downhole fractionation correction (Paton et al., 2010). A long-term, laboratory-specific excess uncertainty of 2% was added in quadrature to isotope ratios obtained after data reduction to better represent inherent uncertainties in the data (method outlined in Horstwood et al., 2016). Concordia diagrams were plotted and weighted mean $^{206}Pb/^{238}U$ dates were calculated using IsoplotR (Vermeesch, 2018).

4.2.3. CA-ID-TIMS

U-Pb dates were obtained by chemical abrasion–isotope dilution–thermal ionization mass spectrometry (CA-ID-TIMS) from analyses of single zircon grains, using the method modified after Mattinson (2005). CL images and LA-ICP-MS data were used to target zircons for TIMS analysis. Selected zircons were removed from the epoxy mounts and chemically abraded. The remaining zircon was spiked with the Boise State University mixed ^{233}U-^{235}U-^{205}Pb tracer solution (BSU-1B). U and Pb were separated from the zircon matrix using an HCl-based anion-exchange chromatographic procedure (Krogh, 1973), eluted together, and dried with 2 µL of 0.05 N H_3PO_4. Pb and U were loaded on a single outgassed Re filament in 5 µL of a silica-gel/phosphoric acid mixture (Gerstenberger and Haase, 1997), and U and Pb isotopic measurements were made on a GV Isoprobe-T multicollector TIMS instrument equipped with an ion-counting Daly detector.

CA-ID-TIMS U-Pb dates and uncertainties were calculated using the algorithms of Schmitz and Schoene (2007), calibration of the BSU-1B tracer solution to $^{235}U/^{205}Pb$ = 77.93 and $^{233}U/^{235}U$ = 1.007066, U decay constants recommended by Jaffey et al. (1971), and $^{238}U/^{235}U$ = 137.818 (Hiess et al., 2012). The $^{206}Pb/^{238}U$ ratios and dates were corrected for initial ^{230}Th disequilibrium using $D_{Th/U}$ = 0.20 ± 0.05 (1 σ) and the algorithms of Crowley et al. (2007), resulting in an increase in the $^{206}Pb/^{238}U$ dates of ~0.09 Ma. A weighted mean $^{206}Pb/^{238}U$ date was calculated from equivalent dates (probability of fit >0.05) using Isoplot 3.0 (Ludwig, 2003) with error at the 95% confidence interval. Errors on dates from individual analyses are at 2σ. Full details of the methodology are provided in Supplemental Material Item A.

5. RESULTS

5.1. Petrography

Modal mineralogy for the Dadeville Complex samples is detailed in Table 1.

5.1.1. Ropes Creek Amphibolite, Waverly Gneiss, and Associated Units in Georgia

Samples mapped as Ropes Creek Amphibolite and associated unnamed units in Georgia (AL20–04, AL20–05, AL20–38, AL20–41, AL20–43, AL20–47, AL22–14, AL22–18, AL22–21, AL22–27, AL22–28, AL22–29, AL22–33, AL22–34) have well-developed foliations defined by aligned amphiboles (Fig. 2A). These units comprise 30–70 modal % fine- to medium-grained amphibole and 20–55 modal % fine- to medium-grained plagioclase, with minor quartz veins and accessory epidote, clinozoisite, ilmenite/magnetite/chromite, and rutile. Samples AL20–06 and AL22–11 had low abundances of plagioclase (5 modal%) due to significant to epidotization (20 modal % epidote). Plagioclase was also variably altered to sericite, with alteration occurring as near-isotropic microcrystalline aggregates that displayed a "stringy" texture (Fig. 2A). Where present, epidote displayed a sieve texture.

The Waverly Gneiss samples (AL22–30, AL22–31, AL22–32, AL22–35) comprised 40–60 modal % amphibole, 10–30 modal % clinopyroxene (excluding AL22–31), and 20–40 modal % plagioclase. Samples AL22–30 and AL22–31 had 10–15 modal % quartz in veins. In these rocks, amphiboles exhibited chemical zonation evidenced by brown-to-green zoning from core to rim (Fig. 2B). These features were also present in three samples collected from sites mapped as Ropes Creek Amphibolite and unnamed amphibolites from Georgia (AL20–38, AL20–41, AL20–47).

5.1.2. Doss Mountain

Most rocks from the mapped Doss Mountain suite (AL20–23, AL20–24, AL20–26, AL20–27, AL20–28, AL20–29, AL20–30) exhibited no foliation. They comprised 25–90 modal % medium- to coarse-grained (up to 5 mm) pyroxene and 30–70 modal % medium-grained (up to 2 mm) plagioclase, with accessory ilmenite, rutile, zoisite, antigorite, garnet, and spinel. Pyroxenes showed alteration of varying degrees to fine-grained (<1 mm) amphibole, and plagioclase exhibited complex polysynthetic twinning (Fig. 2C). Sample AL20–24 comprised only pyroxene with ~10 modal % alteration to amphibole. Four Doss Mountain samples (AL20–23, AL20–27, AL20–29, AL20–30) contained both orthopyroxene and clinopyroxene and had garnet coronae developed between plagioclase and amphibole. Two samples differed significantly from the rest of the Doss Mountain rocks; AL22–26 shared petrographic characteristics with the Ropes Creek Amphibolite, and AL20–45 was comparable to the Waverly Gneiss.

5.1.3. Intrusive Mafic-Ultramafic Rocks

Twelve samples were collected from units mapped as intrusive mafic-ultramafic rocks, and all but AL20–32 displayed characteristics resembling either the Doss Mountain samples or the

TABLE 1. MODAL (%) MINERAL PROPORTIONS FOR DADEVILLE COMPLEX SAMPLES

Sample	Latitude (°N)	Longitude (°W)	Opx	Cpx	Amph	Plag	Qtz	Gar	Ep	Serp	Other
AL20-01	32.85	85.17			70	20	10	<1			
AL20-04	32.83	85.34			60	40			<1		
AL20-05	32.83	85.34			70	30					
AL20-06	32.83	85.34			75	5			20		
AL20-15	32.74	85.76			65	30			5		
AL20-19	32.93	85.48			50	50					
AL20-20	32.93	85.48	10	80	<1	10					
AL20-23	32.86	85.66			45			<1	20	30	
AL20-24	32.86	85.66	90		10						
AL20-26	32.86	85.66	50	5	5	35		<1		5	
AL20-27	32.86	85.66	10	20	5	40		5		5	
AL20-28	32.86	85.66			40	40		20			
AL20-29	32.85	85.66	35		25	40					
AL20-30	32.85	85.65	15	15	30	40		<1			
AL20-31	32.93	85.63		25	25	50					
AL20-32	32.90	85.66	15	15	30	35					Olivine + biotite
AL20-35	32.73	85.77			60	35	<1	3			Clinozoisite
AL20-36	32.82	85.65	30		30	40					
AL20-37	32.81	85.66	20	70	10						
AL20-38	32.74	85.48			50	20	15	10	<1	<1	Biotite
AL20-41	32.61	85.69			55	35			10		
AL20-43	32.78	85.67			70	25			5		
AL20-45	32.87	85.64			60	40			<1		
AL20-47	32.95	85.18			50	50					
AL22-04	32.93	85.66			50	45			5		
AL22-05	32.93	85.66			55	45					
AL22-07	32.94	85.63			55	40			5		
AL22-11	33.03	85.14		5	65	5	5		20		
AL22-14	32.73	85.79			60	30	5		5		
AL22-18	32.66	85.66			60	30	10				
AL22-21	32.70	85.60			60	30	5		5		
AL22-26	32.86	85.66			70	30					Chlorite
AL22-27	32.77	85.45			40	50	10				
AL22-28	32.77	85.45			50	35	15			<1	
AL22-29	32.75	85.40			40	20	20		20		
AL22-30	32.78	85.39		10	40	40	10				
AL22-31	32.88	85.35			45	40	15				Talc
AL22-32	32.81	85.34		30	50	20					
AL22-33	32.92	85.16	5	10	30	55					
AL22-34	33.08	85.22			65	35					
AL22-35	32.92	85.32		10	60	30					

Notes: Opx—orthopyroxene; Cpx—clinopyroxene; Amph—amphibole; Plag—plagioclase; Qtz—quartz; Gar—garnet; Ep—epidote; Serp—serpentine.

Ropes Creek Amphibolite and associated unnamed amphibolites. Six of the samples shared characteristics with the Doss Mountain samples (AL20–15, AL20–19, AL20–20, AL20–31, AL20–36, AL20–37), including coarse-grained plagioclase with complex polysynthetic twinning and alteration of primary pyroxenes to fine-grained amphibole. Five samples (AL20–01, AL20–35, AL22–04, AL22–05, AL22–07) displayed "stringy" plagioclase alteration and well-developed foliation defined by aligned amphiboles, which resembled the Ropes Creek Amphibolite and associated unnamed amphibolite units from Georgia. Sample AL20–32 from the Easton Complex was unique in the sample set by consisting of relict grains of pyroxene that had been significantly altered to amphibole, having biotite present as small alteration patches within the amphiboles, and having two observed grains of olivine in thin section.

5.2. Bulk-Rock Geochemistry

As described above, the mapped units in the Dadeville Complex displayed different petrographic textures and mineralogical compositions (Section 5.1). This section therefore subdivides samples according to rock description into group A (fine- to medium-grained, foliated, mafic-to-intermediate) and group B (medium-grained, nonfoliated, mafic) samples. In the sections below, the whole-rock major- and trace-element geochemistry of the Dadeville Complex samples is compared to that of the Izu-Bonin-Mariana forearc oceanic crust lavas (Ishizuka et al., 2011; Pearce and Reagan, 2019; Reagan et al., 2010, 2015; Shervais et al., 2021). Complete whole-rock geochemistry is detailed in Table 2.

5.2.1. Major Elements

Group A samples, which contained 3–18 wt% MgO, 43–56 wt% SiO_2, 0.1–3 wt% TiO_2, 4–20 wt% Al_2O_3, 5–19 wt% Fe_2O_3, 6–17 wt% CaO, ≤3.24 wt% Na_2O, and <0.9 wt% K_2O, generally showed significant overlap with the forearc rocks from the Izu-Bonin-Mariana but typically with lower SiO_2 and

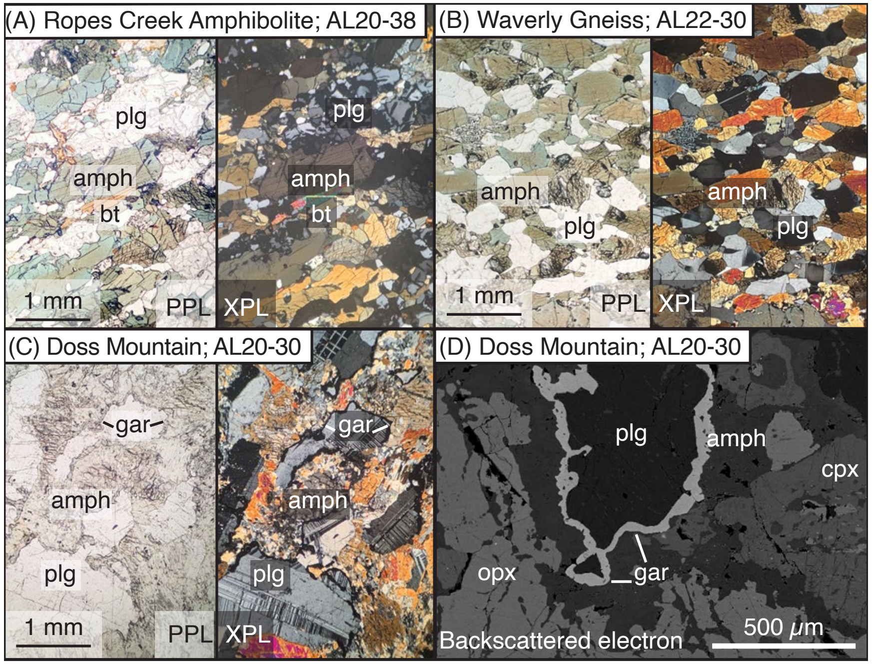

Figure 2. Photomicrographs of Dadeville Complex rocks showing distinctive mineral assemblages and textures. (A) Ropes Creek Amphibolite with "stringy" alteration texture (extinct in cross-polarized light [XPL]) of plagioclase. (B) Waverly Gneiss with zoning in amphiboles expressed as brown-to-green variation from cores to rims. (C) Doss Mountain granulite sample displaying complex twinning in plagioclase crystals and alteration of pyroxenes (first-order gray birefringence in XPL) to fine-grained amphibole (second-order orange to pink in XPL). Extinct rims (XPL) on plagioclase crystals are garnet coronae. (D) Backscattered electron image of Doss Mountain granulite sample showing garnet corona (light gray) on plagioclase crystal (dark gray). Abbreviations: amph—amphibole; bt—biotite; cpx—clinopyroxene; gar—garnet; opx—orthopyroxene; plg—plagioclase feldspar; PPL—plane-polarized light.

Na_2O values (Fig. 3A). Relative to group A samples, group B samples showed higher concentrations of MgO (5–26 wt%), lower concentrations of TiO_2 (<1 wt%), and overlapping concentrations of all other elements. Group B samples also showed significant overlap with the Izu-Bonin-Mariana data, but they typically exhibited slightly higher MgO and CaO contents and slightly lower SiO_2, Na_2O, K_2O, and P_2O_5 contents (Fig. 3A). The Dadeville Complex samples (except one) plot along the tholeiitic trend (Fig. 3D) on the alkalis-iron-magnesium (AFM) volcanic classification diagram (Irvine and Baragar, 1971).

5.2.2. Trace Elements

The high field strength elements (HFSEs; Nb, Ta, Zr, and Hf), generally considered to be immobile during metamorphism and secondary alteration, are plotted against MgO (wt%) in the bivariate diagrams of Figure 3B. The Zr concentrations of group A samples span a large range, (1.39–298.78 ppm) with most having >25 ppm, while Zr concentrations of group B samples are lower (<10 ppm), with three exceptions (AL22–34, AL22–32, and AL20–30), which range 39.42–90.78 ppm. The Hf concentrations follow the same pattern as for Zr, with the group A samples having concentrations of 0.08–7.32 ppm, with most >0.28, and the group B samples having ≤0.34 ppm, with the exception of the same samples (AL22–34, AL22–32, and AL20–30), which range 1.21–2.18 ppm. The Nb concentrations for group A samples range 0.14–4.47 ppm, except for sample AL20–45 (20.73 ppm), while group B samples contain 0.02–4.17 ppm Nb. The Ta concentrations for group A samples range 0.01–0.33 ppm, except for sample AL20–45, which has a Ta concentration of 1.13 ppm. Group B samples contain 0–0.28 ppm Ta.

Figure 3C plots ratios of selected rare earth elements (REEs) against MgO (wt%). Group A samples have positive to negative heavy REE (HREE) slopes ($[Gd/Lu]_{N\text{-MORB}}$ = 0.83–1.86, where N-MORB denotes normal mid-ocean-ridge basalt), positive to negative light REE (LREE) slopes ($[La/Sm]_{N\text{-MORB}}$ = 0.69–4.05), and a range from positive to negative slopes across all REEs ($[La/Lu]_{N\text{-MORB}}$ = 0.63–7.51). The group B samples have positive to negative HREE slopes ($[Gd/Lu]_{N\text{-MORB}}$ = 0.6–2.42), negative LREE slopes ($[La/Sm]_{N\text{-MORB}}$ = 1.13–4.21), and negative slopes across all REEs ($[La/Lu]_{N\text{-MORB}}$ = 1.21–6.73).

5.3. Geochronology

5.3.1. LA-ICP-MS

LA-ICP-MS uncertainties provided below are 2s (sample standard deviation; after Horstwood et al., 2016). Three amphibolites yielded zircons for U-Pb analysis (Fig. 4). Two of the amphibolites (AL20–35 and AL22–14) were sampled ~2 km apart in the SW corner of the complex, with one collected from an area mapped as Ropes Creek Amphibolite and the other from part of the unnamed mafic-ultramafic rock unit (Fig. 1B). The zircons from AL20–35 were 100–200 μm and euhedral to subhedral, displayed oscillatory, sector, patchy, and/or spongy zoning, and had Th/U values of 0.16–0.22. LA-ICP-MS analysis of zircons from this sample yielded a 454.76 ± 3.55 Ma (2s) weighted mean $^{206}Pb/^{238}U$ date (*n* = 13; mean square weighted deviation [MSWD] = 1.1). The AL22–14 zircons were 200–400 μm, commonly fractured, and euhedral to anhedral, and

TABLE 2. WHOLE ROCK MAJOR- AND TRACE-ELEMENT ANALYSES FOR DADEVILLE COMPLEX SAMPLES

Sample ID	AL20-01	AL20-04B	AL20-05	AL20-06	AL20-15	AL20-19	AL20-20	AL20-23	AL20-24	AL20-26	AL20-27	AL20-28	AL20-29	AL20-30	AL20-31	AL20-32	AL20-35	AL20-36	AL20-37	AL20-38	AL20-41	AL20-43	AL20-45	AL20-47	AL22-04	AL22-05	AL22-07	AL22-11	AL22-14	AL22-18	AL22-21	AL22-26	AL22-27	AL22-28	AL22-29	AL22-30	AL22-31	AL22-32	AL22-33	AL22-34	AL22-35
Latitude (°N)	32.85	32.83	32.83	32.83	32.74	32.93	32.93	32.86	32.86	32.86	32.86	32.86	32.85	32.85	32.93	32.90	32.73	32.82	32.81	32.74	32.61	32.78	32.87	32.95	32.93	32.93	32.94	33.03	32.73	32.66	32.70	32.86	32.77	32.77	32.75	32.78	32.88	32.81	32.92	33.08	32.92
Longitude (°W)	85.17	85.34	85.34	85.34	85.76	85.48	85.48	85.66	85.66	85.66	85.66	85.66	85.66	85.65	85.63	85.66	85.77	85.65	85.66	85.48	85.69	85.67	85.64	85.18	85.66	85.66	85.63	85.14	85.79	85.66	85.60	85.66	85.45	85.45	85.40	85.39	85.35	85.34	85.16	85.22	85.32
X-ray fluorescence analyses (wt%)																																									
SiO_2	47.89	53.01	48.28	45.01	49.05	49.66	51.79	44.05	53.9	48.95	46.74	43.96	47.52	49.56	44.88	46.84	54.56	43.75	51.65	50.28	49.28	46.73	45.69	56.37	46.09	42.55	48.49	46.87	48.93	55.65	49.59	47.29	56.38	48.63	48.89	48.56	51.46	50.5	44.89	54.33	49.33
TiO_2	0.74	1.54	0.92	0.8	0.11	0.14	0.16	0.6	0.11	0.26	0.29	0.74	0.36	0.11	0.63	0.82	0.53	0.33	0.14	1.04	1.17	0.36	3.18	0.68	0.61	1.12	0.3	1.06	0.45	0.84	1.7	0.29	0.12	3.1	0.84	1.15	1.04	0.86	0.66	0.49	1.32
Al_2O_3	16.83	13.61	16.17	16.57	18.52	17.71	4.62	17.05	3.98	10.25	17.06	21.49	15.28	15.07	17.69	19.51	17.45	19.21	4.15	17.81	14.74	16.76	13.9	15.07	18.06	19.11	17.23	12.7	16.6	17.66	14.61	17.84	17.98	16.68	15.22	15.43	15.03	7.96	17.62	15.86	14.66
$Fe_2O_3^T$	13.8	13.69	10.34	9.62	4.93	5.97	9.86	14.39	10.66	13.82	11.22	14.24	13.05	9.48	14.87	7.66	11.83	14.78	10.94	12.62	11.97	13.19	18.27	8.92	12.97	17.41	9.19	11.3	14.04	10.24	13.51	10.59	6.15	18.74	9.87	11.34	15.82	10.36	15.11	9.46	11.61
MnO	0.21	0.22	0.24	0.22	0.11	0.11	0.2	0.2	0.2	0.25	0.17	0.24	0.2	0.18	0.2	0.11	0.16	0.15	0.21	0.25	0.19	0.21	0.28	0.22	0.21	0.22	0.16	0.37	0.22	0.16	0.21	0.18	0.13	0.24	0.17	0.17	0.18	0.17	0.24	0.18	0.18
MgO	7.11	5.92	9.62	4.97	10.81	10.95	17.41	8.68	25.83	15.86	10.27	6.07	10.39	12.41	7.04	10.72	3.16	7.43	17.42	6.48	7.88	7.91	4.88	7.45	8	6.1	9.87	8.58	6.83	5.46	7.34	9.63	6.54	5.13	7.72	8.27	4.74	12.96	7.61	6.34	7.41
CaO	11.51	8.58	10.6	21.69	15.25	14.65	15.68	13.64	4.99	10.27	14.17	12.54	12.43	13.02	13.32	10.78	9.76	14.16	14.63	9.01	12.51	12.82	10.87	8.36	12.7	12.69	13.21	16.5	11.25	7.32	10.52	13.72	10.78	6.17	13.95	11.36	9.27	15.59	13.19	10.43	12.35
Na_2O	1.13	3.24	3.14	0.63	0.52	0.52	0.14	0.64	0.16	0.2	0.32	0.51	0.57	0.39	0.99	2.35	1.8	0.33	0.26	1.92	2.37	1.06	1.75	2.95	0.96	0.91	0.89	1.71	1.29	1.9	2.2	0.47	1.26	1.43	2.74	3.23	1.62	1.52	0.8	2.05	2.84
K_2O	0.38	0.07	0.26	0.12	0.28	0.04	0.02	0.22	0.03	0.01	0.01	0.07	0.04	0.04	0.04	0.35	0.17	0.03	0.05	0.68	0.08	0.71	0.87	0.15	0.09	0.09	0.14	0.31	0.34	0.27	0.25	0.06	0.17	0.16	0.21	0.27	0.41	0.4	0.02	0.82	0.11
P_2O_5	0.05	0.1	0.03	0.05	0	0	0	0.02	0	0	0	0.07	0.02	0	0.02	0.09	0.14	0.01	0.02	0.22	0.07	0.04	0.61	0.08	0.04	0.03	0.02	0.07	0.04	0.06	0.15	0.01	0.01	0.3	0.06	0.07	0.07	0.06	0.07	0.08	0.1
Total	99.65	99.98	99.6	99.68	99.58	99.75	99.88	99.49	99.86	99.87	100.25	99.93	99.86	100.26	99.68	99.23	99.56	100.18	99.47	100.31	100.26	99.79	100.3	100.25	99.73	100.23	99.5	99.47	99.99	99.56	100.08	100.08	99.52	100.58	99.67	99.85	99.64	100.38	100.21	100.04	99.91
LOI	0.86	0.21	1.91	0.74	1.36	1.18	0.15	2.28	1.6	–0.04	0.16	0.54	0.35	0.3	0.44	0.35	0.45	0.25	0.43	5.63	0.6	0.81	1.77	2.44	1.62	0.51	1.15	0.99	0.98	4.7	1.98	1.64	1.4	5.97	0.62	0.5	0.79	0.4	0.11	0.94	0.65
XRF analyses (ppm)																																									
Sr	112	104	93	322	92	68	6	65	4	47	85	144	87	75	93	428	109	70	14	61	116	62	94	60	104	125	92	129	72	60	88	80	105	12	113	117	141	69	103	161	124
Zr	13	58	32	0	5	7	10	0	7	4	0	0	3	5	0	47	0	0	10	81	43	2	231	45																	
Cr	0	0	283	201	887	202	975	18	1892	852	3	0	251	292	0	255	0	0	921	37	181	0	0	156				257			75		103		292	288		1472		64	93
V	437	348	254	286	102	136	265	492	125	352	374	372	350	161	501	122	255	576	270	316	297	359	542	226	362	590	225	293	461	292	406	344	135	471	257	305	334	385	437	245	354
LA-ICP-MS analyses (ppm)																																									
P	153.35	516.67	235.61	–70.2	–91.45	42.63	59.85	116.62	10.54	10.59	70.4	124.45	372.11	511.56	135.62	1.01	63.69	55.47	1051.59	156.34	479.8	1498.32	2515.66	219.78	188.4	145.17	77.43	321.13	418.66	268.51	620.37	26.99	62.94	1337.82	268.02	304.49	313.59	239.04	314.56	374.2	347.24
Sc	48.02	36.24	46.32	53.92	32.91	105.93	38.09	56.47	13.35	37.54	81.41	57.74	33.94	23.94	58.22	44.75	60.9	50.5	65.14	40.28	49.6	60.3	39.41	29.03	49.75	50.22	49.64	40.7	61.71	37.51	50.34	54.68	39.49	50.07	42.57	43.51	51.43	73.05	57.69	52.75	43.5
V	290.5	362.94	423.21	177.46	116.09	405.16	130.38	519.64	52.4	287.86	527.23	384.43	392.82	155.99	521.55	146.72	194.08	603.22	406.78	267.69	335.03	462.56	517.86	198.03	305.28	490.94	203.72	260.97	440.95	255.94	335.35	293.14	124.54	365.6	228.77	268.56	276.37	330.59	371.43	239.25	253.79
Cr	401.97	239.32	95.43	206.2	915.73	5829.53	142.36	139.06	97.34	70.34	1282.67	359.6	82.76	389.88	82.19	306.51	674.32	96.98	18.42	42.45	326.88	195.14	34.45	181.9	39.14	19.66	80.89	319.31	78.76	68.23	165.41	65.54	178.1	62.6	357.85	363.21	28.43	1351.48	33.89	161.8	150.17
Mn	1858.45	1824.82	1422.61	1429.52	801.41	4326.06	1062.62	1509.32	304.86	895.12	2549.43	1498.05	1735.66	1031.43	1506.74	1100	1065.99	1175.38	1824.76	1090.44	2513.97	2561.86	2385.9	995.19	0	0	0	0	1678.57	0	0	78.92	159.42	159.42	80.49	0	0	0	0	562.57	1122.1
Co	68.23	43.51	51.98	59.15	53.73	221.51	46.13	50.19	15.55	40.13	111.19	65.13	52.1	71.14	54.93	48.4	39.47	55.08	67.35	46.34	82.8	90	45.38	36.85	48.75	56.43	51.96	46.04	58.23	50.07	46.84	46.98	55.32	60.55	54.47	48.41	40.52	52.66	55.2	67.33	43.31
Ni	181.14	92.35	122.01	125.49	123.99	1236.07	105.26	97.46	50.11	82.08	248.6	153.69	78.04	244.59	66.73	103.87	99.95	117.44	48.7	46.18	125.42	112.43	68.86	82.98	33.62	30.04	49.67	113.16	34.44	29.54	59.89	40.19	88.04	33.21	110.26	82.77	41.1	143.01	33.86	67.44	50.67
Cu	88.78	40.89	54.98	61.45	62.14	162.55	150.14	85.09	22.09	79.28	64.06	133.15	38.76	52.6	81.03	61.91	33.89	212.89	89.98	82.29	46.76	145.7	164.85	59.15	46.8	55.21	51.94	23.32	100.73	13.49	69.31	32.14	19.07	74.02	10.16	12.61	15.27	17.27	46.57	26.28	30.44
Zn	44.73	146.16	98.81	50.77	27.83	202.18	185.06	86.96	12.22	43.37	117.81	87.06	66.46	58.53	97.06	49.7	40.43	56.72	150.38	61.76	192.35	129.57	299.52	90.7	78.05	87.13	51.69	76.4	122.75	62.59	112.92	63.52	38.96	76.23	85.1	67.35	59.59	102.7	88.3	73.19	62.76
Rb	3.09	1.18	5.29	16.87	9.32	1.42	18.44	22.06	0.44	0.54	2.88	1.61	3.11	10.78	0.89	1.25	1.93	1.08	4.74	3.88	5.61	12.05	5.55	1.42	3.59	1.9	3.63	7.07	8.9	4.31	3.4	1.61	2.54	1.62	3.94	6.21	8.28	3.63	0.88	17.29	1.16
Sr	131.49	131.66	139.38	106.32	106.92	37.96	76.95	93.55	28	83.14	98.76	125.49	195.22	615.9	130.98	80.15	16.92	101.06	223.46	60.84	114.14	121.94	125.84	94.48	130.78	164.97	112.94	161.06	99.86	77.2	115.1	96.4	121.16	30.33	144.4	147.96	181.92	85.52	140.06	219.73	132.89
Y	21.09	25.01	6.96	4.45	2.31	9.11	3.85	5.07	1.47	1.51	4.15	6.26	3.02	15.26	6.59	2.55	3.37	1.16	24.73	6.97	23.35	41.42	51.27	15.1	8.41	5.72	9.67	37.96	18.34	40.29	40.02	3.89	11.18	67.1	23.56	29.15	31.45	23.1	10.59	26.26	32.51
Zr	47.06	61.13	26.08	5.51	2.78	8.52	7.74	1.01	1.46	1.18	2.76	8.83	6.32	90.78	6.36	3.49	3.64	1.56	31.86	3.22	69.94	152.83	298.78	36.24	4.89	1.39	8.18	56.5	33.94	101.26	101.99	3.82	29.29	210.22	42.84	61.53	37.83	63.07	3.8	39.42	59.1
Nb	1.14	1.64	2.18	0.25	0.25	0.3	0.2	0.07	0.02	0.02	0.04	0.42	0.45	4.17	0.25	0.1	1.19	0.26	3.91	0.3	2.32	4.36	20.73	0.78	0.54	0.14	0.66	2.41	2.98	2.29	2.36	0.16	1.17	4.47	0.64	1.41	1.54	2.82	0.5	1.94	1.27
Cs	0.04	0.1	0.03	0.86	0.18	0.12	0.86	0.63	0.03	0.17	0.2	0.08	0.11	0.41	0.08	0.15	0.07	0.29	0.14	0.09	0.42	0.22	0.26	0.03	0.17	0.1	0.39	0.22	0.19	0.05	0.18	0.03	0.09	0.04	0.18	0.1	0.19	0.1	0.06	0.12	0.03
Ba	145.56	18.84	54.35	32.87	38.89	12.39	37.76	65.07	9.86	3.83	41.62	26.94	20.04	97.94	15.23	17.33	40.26	7.96	60.79	5.74	92.22	350.56	119.11	8.53	27.65	6.43	17.79	104.1	65.79	72.51	83.59	19	43.61	26.45	33.92	39.01	140.96	67.56	9.33	226.52	14.23
La	3.32	3.47	5.06	2.01	0.7	1.46	1.25	3.1	0.46	0.23	0.81	2.49	2.52	6.54	1.87	0.72	2.22	0.55	8.91	1.35	7.67	19.52	33.44	1.27	2.17	0.83	3.17	4.71	5.45	7.97	4.26	0.74	3.94	8.78	1.31	2.7	6.75	9.4	1.98	9.3	3.97
Ce	9.34	10.29	12.15	3.53	1.38	3.05	2.29	1.09	1.08	0.67	1.65	6.02	4.91	16.56	4.46	1.81	3.4	1.26	23.82	4.33	17.21	36.51	71.77	4.15	5.64	1.93	4.95	13.05	14.93	17.95	15.22	1.99	12.7	23.81	3.74	6.66	10.25	26.45	5.44	20.01	6.93
Pr	1.45	1.81	1.56	0.56	0.26	0.56	0.39	0.96	0.14	0.1	0.3	0.87	0.59	2.17	0.69	0.26	0.58	0.17	3.58	0.74	2.46	7.11	9.71	0.79	0.8	0.36	0.92	1.88	2.38	3.99	2.19	0.32	1.19	4.14	0.87	1.36	2.43	4.33	0.94	2.85	1.74
Nd	7.44	8.66	6.29	2.41	1.08	2.8	1.92	3.73	0.63	0.61	1.6	4.02	2.57	10.44	3.65	1.41	2.45	0.77	17.25	3.78	11.2	30.41	40.89	4.6	4.23	2.24	4.2	9.96	10.81	18.26	11.85	1.73	5.04	21.9	5.36	7.61	11.83	21.83	5.04	12.56	9.01
Sm	2.46	3.03	1.42	0.56	0.25	0.99	0.58	1.03	0.2	0.22	0.58	1.16	0.63	2.6	1.09	0.46	0.59	0.21	4.53	1.08	3.2	8.22	10.25	1.57	1.29	0.75	0.94	3.51	3.29	4.99	4.17	0.59	1.46	7.06	1.96	2.8	3.7	5.7	1.64	3.35	3.09
Eu	0.95	1.2	0.58	0.29	0.17	0.29	0.26	0.39	0.09	0.11	0.22	0.38	0.58	1.08	0.43	0.16	0.14	0.11	1.19	0.32	1.2	2.35	2.84	0.66	0.55	0.62	0.42	1.2	0.66	1.21	1.42	0.22	0.26	2.28	0.78	0.98	1.06	1.38	0.6	0.85	1.21
Gd	3.18	3.98	1.43	0.5	0.46	1.05	0.57	0.99	0.21	0.26	0.65	1.14	0.59	2.82	1.29	0.51	0.59	0.21	4.52	1.15	3.82	8.06	9.53	2.11	1.53	0.99	1.38	4.96	3.32	5.88	6.25	0.66	1.45	9.24	3.24	3.87	4.35	5.7	1.76	3.68	4.46
Tb	0.57	0.78	0.22	0.1	0.06	0.19	0.11	0.18	0.04	0.04	0.12	0.19	0.09	0.47	0.21	0.08	0.09	0.03	0.74	0.2	0.69	1.31	1.57	0.41	0.25	0.19	0.24	0.84	0.51	1.04	1.02	0.11	0.31	1.68	0.58	0.71	0.71	0.84	0.29	0.58	0.81
Dy	3.83	4.63	1.4	0.72	0.42	1.51	0.68	1.17	0.31	0.3	0.78	1.21	0.56	2.97	1.37	0.52	0.54	0.23	4.59	1.27	4.28	8.73	10.01	2.69	1.47	1.15	1.37	5.72	2.97	6.59	6.68	0.71	1.77	11.26	3.8	4.77	4.9	4.55	1.94	4.04	5.32
Ho	0.82	0.98	0.28	0.18	0.09	0.34	0.14	0.23	0.06	0.06	0.17	0.26	0.12	0.61	0.28	0.11	0.13	0.05	0.97	0.27	0.95	1.88	2.07	0.6	0.34	0.24	0.33	1.28	0.67	1.47	1.48	0.15	0.36	2.44	0.85	1.01	1.1	0.87	0.42	0.86	1.17
Er	2.45	2.8	0.86	0.47	0.26	1.16	0.4	0.67	0.19	0.19	0.48	0.71	0.36	1.74	0.82	0.32	0.38	0.12	2.82	0.84	3.04	5.48	5.85	1.6	0.93	0.71	0.9	3.85	1.99	4.66	4.51	0.45	1.24	7.34	2.5	3.09	3.25	2.36	1.18	2.72	3.5
Tm	0.34	0.44	0.12	0.05	0.04	0.17	0.07	0.1	0.02	0.03	0.08	0.11	0.05	0.22	0.11	0.04	0.05	0.02	0.42	0.12	0.43	0.84	0.84	0.26	0.14	0.1	0.13	0.55	0.28	0.74	0.66	0.06	0.19	1.12	0.38	0.45	0.46	0.34	0.17	0.4	0.5
Yb	2.39	3.06	0.85	0.58	0.36	1.38	0.49	0.69	0.17	0.2	0.54	0.77	0.4	1.48	0.78	0.34	0.36	0.16	2.82	0.89	3.17	6.44	5.96	1.71	0.94	0.69	0.92	3.66	2.28	5.31	4.38	0.39	1.33	9.64	2.52	2.86	2.9	1.99	1.08	2.93	3.26
Lu	0.36	0.45	0.13	0.07	0.03	0.22	0.06	0.1	0.03	0.03	0.08	0.11	0.07	0.23	0.13	0.05	0.06	0.03	0.42	0.14	0.44	0.95	0.81	0.24	0.14	0.08	0.14	0.54	0.34	0.86	0.88	0.07	0.22	1.34	0.37	0.44	0.47	0.29	0.16	0.43	0.5
Hf	1.4	2.02	0.78	0.29	0.13	0.3	0.21	0.05	0.06	0.06	0.16	0.34	0.17	2.04	0.26	0.14	0.13	0.05	1.23	0.18	2.07	4.34	7.32	1.1	0.19	0.08	0.28	1.76	1.44	3.29	3.03	0.18	0.93	6.04	1.32	1.87	1.44	2.18	0.2	1.21	1.72
Ta	0.08	0.15	0.13	0.04	0.02	0.03	0.05	0.01	0	0.01	0.02	0.03	0.02	0.28	0.02	0.01	0.06	0.02	0.17	0.01	0.23	0.25	1.13	0.08	0.08	0.04	0.09	0.15	0.19	0.15	0.19	0.03	0.09	0.33	0.07	0.17	0.11	0.14	0.05	0.13	0.11
Pb	2.67	11.63	2.62	5.94	2.63	1.32	6.97	1.46	0.32	0.39	0.57	1.45	1.28	1.55	1.14	1	0.66	0.99	4.92	2.99	15.23	3.7	25.21	2.88	1.16	1.01	1.77	6.8	4.62	2.08	2.07	0.79	3.23	3.46	6.04	1.17	3.15	2.7	0.89	4.12	0.78
Th	0.19	0.47	0.36	0.01	0.04	0.08	0.04	0.01	0.03	0.01	0.02	0.12	0.08	0.66	0.03	0.05	0.05	0.03	0.48	0.01	1.98	4.16	2.52	0.07	0.13	0.05	0.25	1.9	1.09	1.51	0.33	0.04	0.54	1.14	0.07	0.18	3.22	0.53	0.05	2.18	0.15
U	0.08	0.14	0.1	0.12	0.07	0.04	0.19	0.01	0.01	0	0.01	0.04	0.02	0.18	0.01	0.02	0.02	0.02	0.25	0.17	0.42	1.04	0.95	0.03	0.04	0.02	0.07	1.93	0.55	0.29	0.29	0.02	0.15	0.22	0.1	0.06	0.43	0.24	0.02	0.54	0.07
Trace-element ratios																																									
$[Gd/Lu]_{N-MORB}$	1.10	1.10	1.34	0.88	1.86	0.60	1.14	1.23	1.00	1.00	1.00	1.24	1.07	1.54	1.30	1.27	1.23	1.00	1.35	1.00	1.07	1.05	1.46	1.08	1.40	1.42	1.27	1.13	1.22	0.84	0.88	1.29	0.83	0.85	1.07	1.08	1.15	2.42	1.33	1.06	1.10
$[La/Sm]_{N-MORB}$	1.41	1.21	3.76	3.81	2.80	1.53	2.27	3.18	2.57	1.13	1.45	2.25	4.21	2.64	1.83	1.71	4.05	2.75	2.07	1.32	2.52	2.50	3.43	0.85	1.78	1.14	3.53	1.42	1.74	1.68	1.08	1.30	2.80	1.31	0.69	1.01	1.91	1.73	1.27	2.93	1.35
$[La/Lu]_{N-MORB}$	1.71	1.42	7.00	5.00	4.00	1.21	3.57	5.64	3.00	1.29	1.78	3.96	6.73	5.22	2.78	2.64	6.85	3.67	3.91	1.74	3.16	3.74	7.51	0.96	2.90	1.74	4.23	1.59	2.95	1.68	0.88	2.14	3.27	1.19	0.63	1.11	2.62	5.88	2.19	3.96	1.45
$[Dy/Yb]_{N-MORB}$	1.06	1.02	1.11	0.84	0.75	0.73	0.94	1.13	1.17	1.00	0.94	1.08	0.92	1.35	1.15	1.00	1.00	1.00	1.10	0.97	0.90	0.91	1.13	1.05	1.03	1.09	1.00	1.05	0.87	0.83	1.03	1.23	0.91	0.78	1.01	1.12	1.14	1.54	1.23	0.93	1.09

Notes: XRF—X-ray fluorescence, LOI—loss on ignition; LA-ICP-MS—laser ablation–inductively coupled plasma–mass spectrometry; N-MORB—normal mid-ocean-ridge basalt.

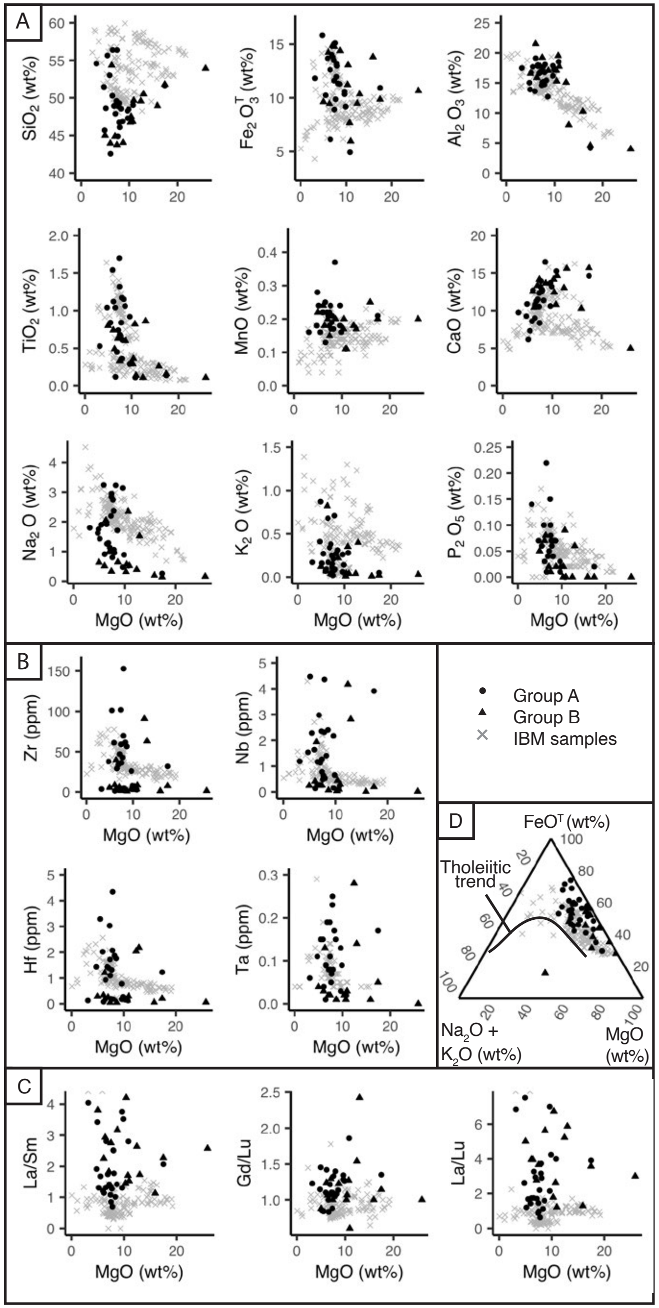

Figure 3. Composition of the Dadeville samples plotted with Izu-Bonin-Mariana (IBM) forearc rocks. (A) Bivariate diagrams of major-element oxides vs. MgO. (B) Bivariate diagrams of high field strength elements (HFSE) vs. MgO. (C) Ratios of select rare earth elements (REE) vs. MgO. (D) Alkalis-iron-magnesium (AFM) volcanic classification diagram (Irvine and Baragar, 1971). IBM values on all plots are from Ishizuka et al. (2011), Pearce and Reagan (2019), Reagan et al. (2010, 2015), and Shervais et al. (2021).

they showed oscillatory, sector, cloudy, or weak zoning in CL, with some also showing thin metamorphic rims. The Th/U of the zircons for AL22–14 ranged 0.12–0.89. LA-ICP-MS analyses of zircons from this sample yielded a 464.87 ± 6.85 Ma (2σ) weighted mean $^{206}Pb/^{238}U$ date (n = 55/56; MSWD = 0.53). A third geochronology sample (AL22–34) was collected from the eastern side of the complex, in Georgia (Fig. 1B). The zircons from AL22–34 were 200–300 µm, fractured, and euhedral to anhedral and showed no, weak, cloudy, or patchy zoning in CL. The AL22–34 zircons had Th/U values of 0.38–1.28. LA-ICP-MS analysis of zircons from this sample yielded a 467.20 ± 16.1 Ma (2σ) weighted mean $^{206}Pb/^{238}U$ date (n = 10; MSWD = 0.52).

5.3.2. CA-ID-TIMS

Eight zircon grains from previously analyzed (by LA-ICP-MS) sample AL20–35 were selected for CA-ID-TIMS analysis. The six oldest grains yielded a weighted mean age of 467.07 ± 0.13 Ma (95% confidence interval; MSWD = 1.5; Fig. 4). This is interpreted to date igneous crystallization. Two resolvable "younger" grains yielded dates of 466.27 ± 0.31 Ma (2σ) and 464.91 ± 0.33 Ma (2σ), which are interpreted to have retained (after chemical abrasion) domains that underwent Pb loss and/or to have small metamorphic rims.

6. DISCUSSION

6.1. Geochemistry

To ensure that tectonomagmatic interpretations were made only on samples appropriate for use with common geochemical discrimination schemes, the meta-igneous Dadeville Complex samples were screened for evidence of significant alteration or compositional deviation from their original melt. This assessment included checks for cumulate effects (section 6.1.1) and postcrystallization mobility of the various elements (section 6.1.2). After screening, geochemical classifications (section 6.1.3) were based on (1) samples considered to be

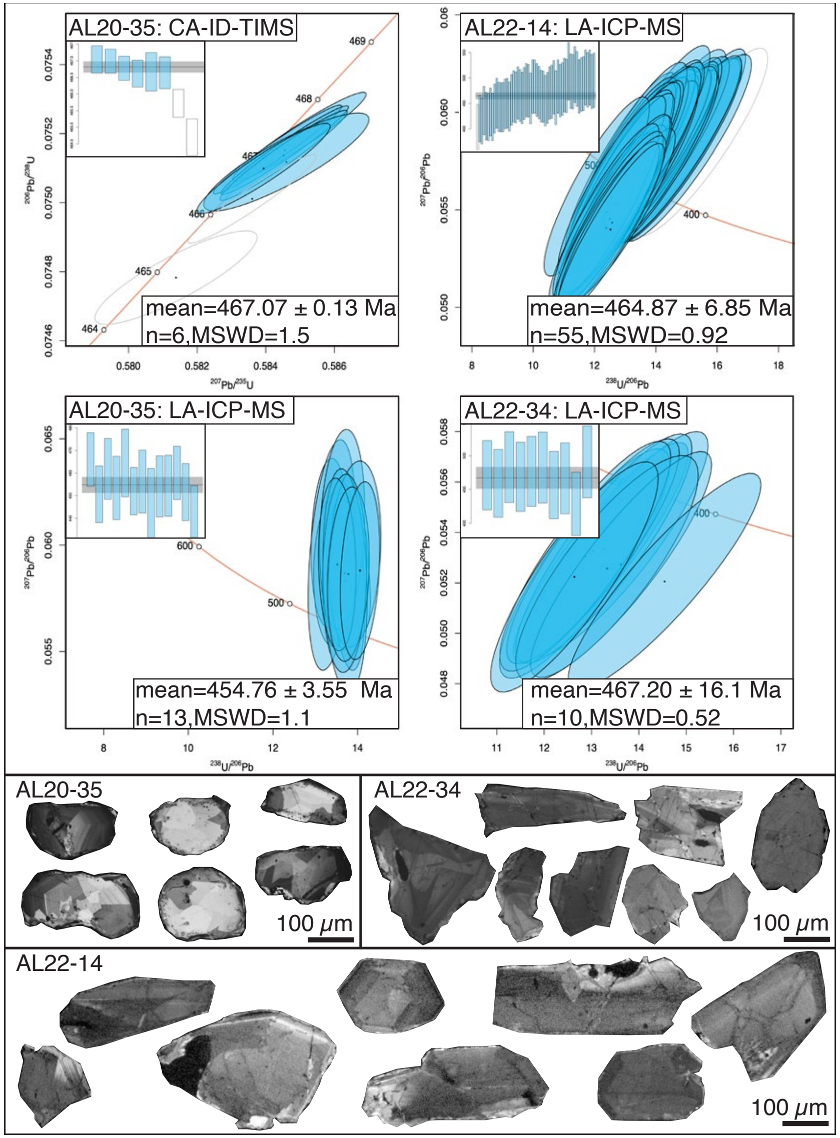

Figure 4. Tera-Wasserburg (laser ablation–inductively coupled plasma–mass spectrometry [LA-ICP-MS]) and Wetherill (chemical abrasion–isotope dilution–thermal ionization mass spectrometry [CA-ID-TIMS]) Concordia diagrams and weighted mean age ($^{206}Pb/^{238}U$) plots (inset) showing U-Pb LA-ICP-MS and CA-ID-TIMS results for zircons from samples AL20–35, AL22–14, and AL22–34. Cathodoluminescence (CL) images of selected grains are also shown for each sample. The two youngest dates obtained by CA-ID-TIMS for AL22–35 are shown in gray outlines and were not included in the age calculation. LA-ICP-MS dates are 2s after Horstwood et al. (2016). Uncertainties on CA-ID-TIMS dates are 95% confidence. MSWD—mean squared weighted deviation.

noncumulate in origin and (2) element groupings with demonstrably limited element mobility during metamorphism/metasomatism.

6.1.1. Cumulate Rocks

Geochemical signatures indicative of formation from cumulate processes were present in some samples collected from the Dadeville Complex. This included prominent positive Eu* anomalies (Eu* = Eu/[Sm + Gd]$^{0.5}$) and low total REE concentrations. Cumulate chemistry is not reflective of magma source; therefore, Eu* anomalies were utilized as a coarse proxy for identifying cumulate effects, and samples with Eu* anomalies <0.7 and >1.1 were not considered for the geochemical classification work outlined in section 6.1.3. Two additional samples with anomalously high Cr (>5000 ppm) and TiO_2 (>3 wt%) values—interpreted to signify accumulation of Ti- and/or Cr-rich minerals via crystal fractionation—were also excluded, leaving 21 samples interpreted as appropriate for use in tectonic interpretations.

6.1.2. Element Mobility

The rocks of the southern Appalachian orogen have experienced postemplacement deformation and metamorphism up to granulite facies and may have experienced subsolidus element mobilization or open-system chemical modification. When using tectonic classification schemes, it is vital to determine whether the elements used have retained their original concentrations or if these elements were mobilized during subsequent metamorphism and/or hydrothermal alteration. To determine the extent of postcrystallization element mobilization within the Dadeville Complex, the samples were evaluated using bivariate diagrams that plot trace elements against the immobile element Y (Fig. 5; method outlined in Guice et al., 2018, 2019). The results showed that the typically fluid-mobile large ion lithophile elements (Ba, Cs, Rb, Sr) had low correlations with Y (R^2 = 0.33, 0.12, 0.27, and 0.29, respectively), indicating that

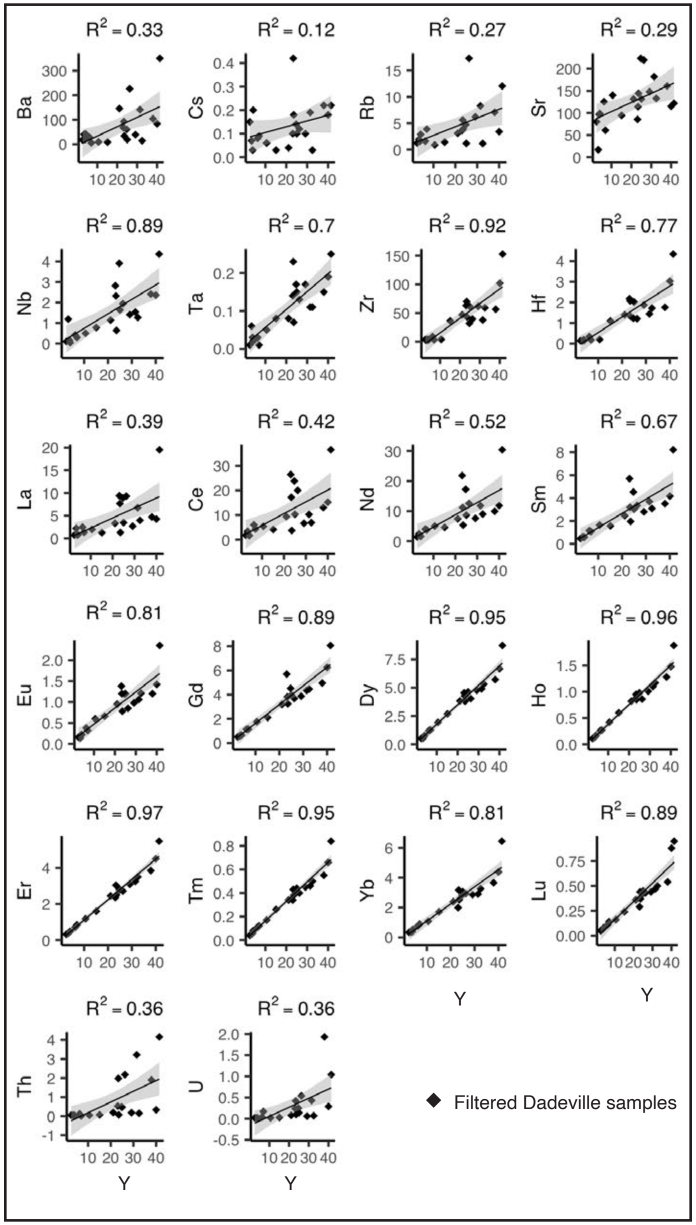

Figure 5. Bivariate diagrams plotting trace elements against the highly immobile element Y (see section 6.1.2. for discussion). Solid lines represent linear regression, and gray bands represent the 95% confidence interval for the fit. R^2 values provided are for the volcanic samples of the Dadeville Complex only (samples that did not pass the cumulate filtering were excluded). All axes are in ppm.

their compositions have likely been altered by secondary processes. The HFSEs (Nb, Ta, Zr, Hf) showed strong correlations (R^2 = 0.89, 0.70, 0.92, and 0.77, respectively), suggesting limited mobility of these elements relative to Y. The LREEs (La, Ce, Pr, Nd, Sm, Eu) also exhibited moderate correlations with Y (R^2 = 0.39–0.81), while the HREEs (Gd, Tb, Dy, Ho, Er, Tm, Yb, Lu) showed strong correlations with Y (R^2 > 0.81), suggesting that these elements were highly immobile relative to Y. Other elements commonly utilized as tectonic discriminators for oceanic basaltic rocks include Th, Ti, V, Mg, and Si. In the Dadeville samples, Th and Ti showed poor correlations with Y (R^2 = 0.36 and 0.19, respectively), and V showed no correlation with Y (R^2 < 0.02). Using Cr as an immobile element proxy for MgO, there was evidence that the Dadeville Complex samples have also experienced secondary Si and Mg mobility (procedure outlined in Pearce and Reagan, 2019). Based on the element mobility analysis, geochemical classification schemes for the Dadeville Complex should be limited to use of the HFSEs and REEs as discriminators of tectonomagmatic setting and evolution.

6.1.3. Geochemical Classification

The volcanic samples from the Dadeville Complex can be subdivided into three groups based on their HFSE and REE characteristics. These groupings are best illustrated with chondrite-normalized REE diagrams and N-MORB–normalized trace-element diagrams (Figs. 6A and 6B). Group 1 (n = 9) samples have features resembling Izu-Bonin-Mariana forearc basalts, with high total HREE values ($\Sigma[\mathrm{Gd–Lu}]_N$ = 9.62–25.86 ppm), depleted LREEs with respect to N-MORB, positive or flat LREE slopes, and flat HREE slopes. Group 2 samples (n = 7) are geochemically comparable to Izu-Bonin-Mariana boninites, showing depleted total HREE values ($\Sigma[\mathrm{Gd–Lu}]_N$ = 1.97–7.00 ppm), negative LREE slopes and flat HREE slopes, and distinctive Nb-Ta and Zr-Hf depletions. We characterize the group 3 samples (n = 2) as island-arc tholeiites, displaying high total HREE values ($\Sigma[\mathrm{Gd–Lu}]_N$ = 15.64–33.69 ppm), negative LREE slopes,

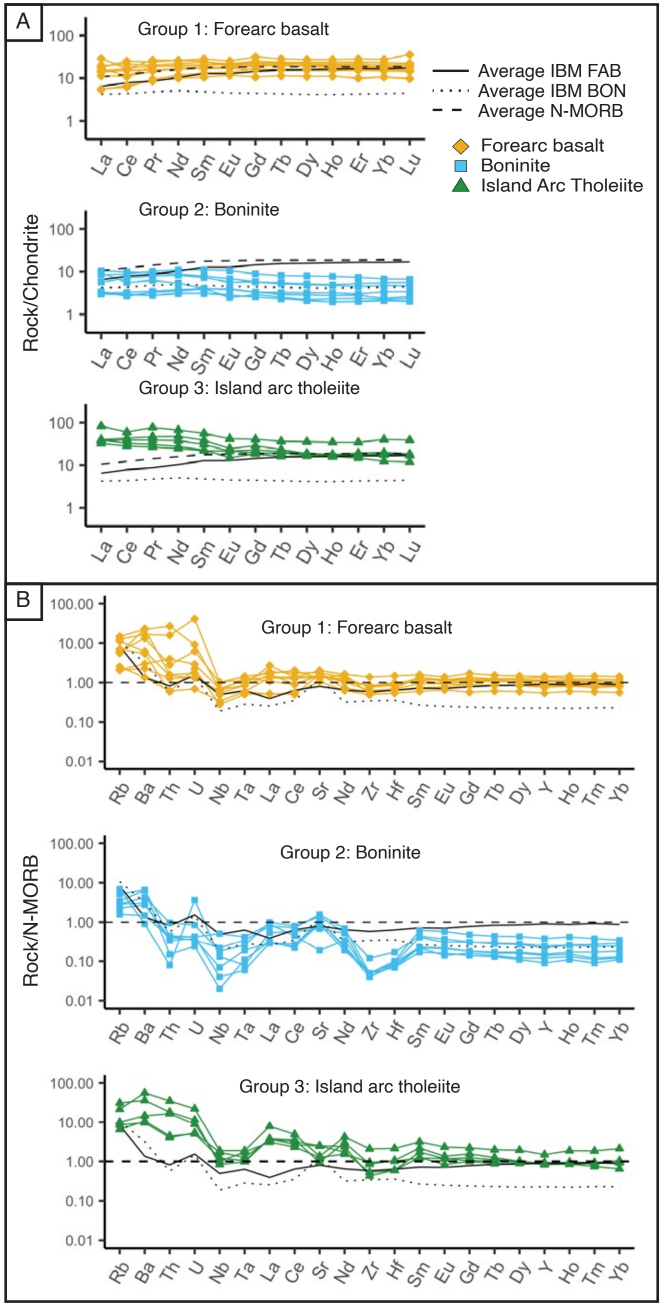

Figure 6. (A) Chondrite-normalized rare earth element (REE) spider diagram with Dadeville Complex samples compared to average forearc basalt (FAB) and boninite (BON) compositions from the Izu-Bonin-Mariana (IBM) forearc. (B) Normal mid-ocean-ridge basalt (N-MORB)–normalized REE spider diagram with Dadeville Complex samples compared to average forearc basalts and boninites compositions from the IBM forearc. IBM average values were calculated from Ishizuka et al. (2011), Pearce and Reagan (2019), Reagan et al. (2010, 2015), and Shervais et al. (2021). Normalizing values are from Sun and McDonough (1989).

and negative overall REE slopes. A volcanic assemblage of forearc basalts, boninites, and island-arc tholeiites suggests that the Dadeville Complex may record subduction initiation and early protoarc development within the Iapetus Ocean (Ishizuka et al., 2011; Reagan et al., 2010, 2019; Pearce and Reagan, 2019; Shervais et al., 2019, 2021; Stern et al., 2012).

6.2. Spatial Distribution

All nine of the forearc basalts samples occur exclusively in the southeastern parts of the Dadeville Complex (Fig. 7). Three of the boninites samples are in the northwestern section, adjacent to Doss Mountain, with the remaining two located in the southeastern section. Three island-arc tholeiite samples are located with the boninites, close to Doss Mountain, three are in the southeastern section, and one is in the northeastern section in Georgia. When compared to findings from the Izu-Bonin-Mariana system, the distribution of geochemistry within the Dadeville Complex volcanics—forearc basalts in the SE to boninites in the NW—suggests that volcanic rocks of the Dadeville Complex may be older (stratigraphically lower) in the southeast and younger (stratigraphically higher) in the northwest. This is consistent with previous interpretations based on structural relationships, which suggested that the northwest section of the Dadeville Complex is structurally higher than the southeast (Tull et al., 2018).

6.3. Timing of Formation of the Dadeville Complex (Relative to the Backarc Wedowee-Emuckfaw-Dahlonega Basin)

Our 467.07 ± 0.13 Ma CA-ID-TIMS U-Pb zircon age from a boninite sample, when combined with the identical LA-ICP-MS U-Pb zircon dates from the two other samples of island-arc tholeiite Ropes Creek Amphibolite (and related units), is interpreted to date forearc/protoarc volcanism in the Dadeville Complex. This 467 Ma date is younger than some previously published LA-ICP-MS U-Pb

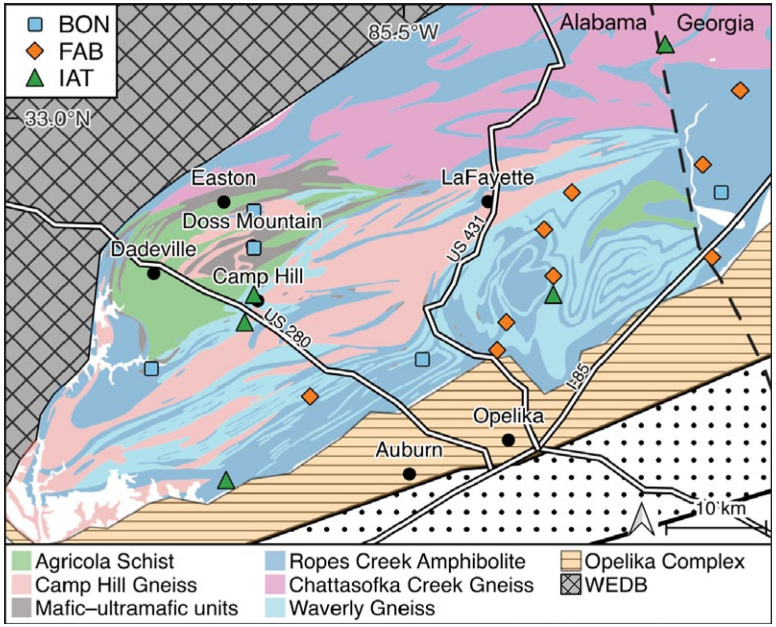

Figure 7. Geologic map of the Dadeville Complex of Alabama and Georgia (modified from Tull et al., 2014) showing lithologic units and distribution of the geochemical groupings from the Dadeville Complex samples. Note that all forearc basalt (FAB) samples are located on the southeast side of the complex, along with two boninite (BON) samples and one island-arc tholeiite (IAT). The other three boninite samples and the other island-arc tholeiite sample are located in the northwest side of the complex. The spatial distribution of the samples suggests an up-stratigraphic evolution in the Dadeville Complex volcanics from oldest in the southeast to youngest in the northwest. WEDB—Wedowee-Emuckfaw-Dahlonega basin.

zircon dates for the Camp Hill Gneiss, Chattasofka Creek Gneiss, Waverly Gneiss, Waresville Formation, and Ropes Creek Amphibolite (Ma et al., 2019; Tull et al., 2018). Each of these previous dates were obtained from felsic units intercalated with or intruding the mafic units that were dated in this study. Previous geochronological interpretations utilized LA-ICP-MS U-Pb zircon dates, which are associated with greater uncertainty than the CA-ID-TIMS approach (e.g., Schaltegger et al., 2015). We interpret the 467.07 ± 0.13 CA-ID-TIMS date to record the early stages of tectonic convergence (subduction initiation and protoarc development in the Iapetus Ocean) in the Alabama-Georgia sector of the southern Appalachians.

Felsic plutonic and extrusive rocks of the Wedowee-Emuckfaw-Dahlonega basin (Fig. 8) are dated at ca. 470–430 Ma (Barineau et al., 2015, 2022; Holm-Denoma and Das, 2010; Ma et al., 2019; McClellan et al., 2007; Thomas, 2001; Tull et al., 2007, 2018), with only one unit—the 482 ± 7 Ma Cane Creek felsic gneiss of the Sally Free Mafic Complex—yielding an anomalously older date (Bream, 2003; Settles, 2002). The 470–430 Ma age range for units of the Wedowee-Emuckfaw-Dahlonega basin is suggestive of initiation of the Wedowee-Emuckfaw-Dahlonega basin backarc soon after the establishment of Dadeville Complex forearc/protoarc at 467 Ma. Cessation of volcanism in the Dadeville Complex and Wedowee-Emuckfaw-Dahlonega basin may have been associated with accretion of the Carolina superterrane, resulting in a regional metamorphic event at ca. 400 Ma (Hibbard, 2000; Ma et al., 2019).

6.4. Granulite-Facies Metamorphism

Although contacts are poorly exposed and generally inferred, the medium-grained, nonfoliated, mafic samples in the Doss Mountain suite and throughout the rest of the Dadeville Complex have previously been interpreted as intrusive to the Ropes Creek Amphibolite (Neilson and Stow, 1986). Petrographic analysis of the Doss Mountain rocks revealed that four of the seven samples contained co-occurring orthopyroxene, clinopyroxene, and coronitic garnet, features suggestive of metamorphic reaction at granulite facies (St-Onge and Ijewliw, 1996). Peak metamorphic conditions in the Dadeville Complex—based on metamorphic mineral assemblages—have been reported as 5–8 kbar and 600–700 °C for the Agricola Schist and 10 kbar and 750–800 °C for the Ropes Creek Amphibolite (Drummond et al., 1997). Microprobe major-element analysis and backscattered-electron (BSE) imaging were performed on six samples that had potential granulite-facies textures (Fig. 2E). Two-pyroxene thermometry using the calibration of Brey and Köhler (1990) provided multiple ranges of temperatures for the samples (see Supplemental Material Item B). The calculations had large errors, and the partition coefficients indicated that the compositions may not be in equilibrium ($KD_{[Fe-Mg]}$ = 0.4–0.8), precluding precise determination of the temperatures reached by the Doss Mountain samples; however, the data indicated that peak pressure-temperature (*P-T*) conditions recorded in the Doss Mountain suite exceeded 7 kbar and 760 °C, consistent with estimates for other units of the Dadeville Complex (Drummond et al., 1997). BSE imaging revealed that the garnet coronae formed at the interface between plagioclase and the amphibolitized rims of clinopyroxene, a texture associated with rehydration of granulite-facies rocks during retrogression to amphibolite-facies assemblages (St-Onge and Ijewliw, 1996). Additionally, garnet was present in some amphibolites sampled from the Ropes Creek Amphibolite, indicating

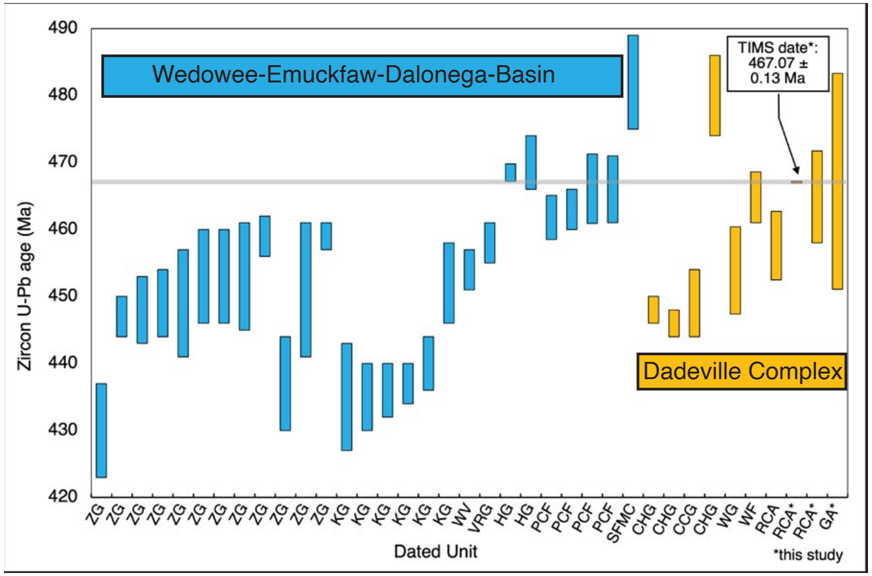

Figure 8. Published laser ablation–inductively coupled plasma–mass spectrometry (LA-ICP-MS) U-Pb zircon ages for units of the Wedowee-Emuckfaw-Dalonega basin (WEDB) and the Dadeville Complex, including the new LA-ICP-MS and chemical abrasion–isotope dilution–thermal ionization mass spectrometry (CA-ID-TIMS) U-Pb zircon dates from this study. Literature data are from Barineau et al. (2015, 2022), Holm-Denoma and Das (2010), Ma et al. (2019), McClellan et al. (2007), Thomas (2001), and Tull et al. (2007, 2018). Gray reference line is for the new CA-ID-TIMS date, which we interpret to represent earliest convergence in the Alabama-Georgia sector of the southern Appalachians. CHG—Camp Hill Gneiss; CCG—Chattasofka Creek Gneiss; GA—unnamed amphibolite from Georgia; HG—Hillabee Greenstone; KG—Kowaliga Gneiss; PCF—Pumpkinvine Creek Formation; RCA—Ropes Creek Amphibolite; SFMC—Sally Free Mafic Complex; VRG—Villa Rica Gneiss; WF—Waresville Formation; WG—Waverly Gneiss; WV—Wedowee metavolcanic; ZG—Zana Granite.

metamorphic pressures exceeding 7 kbar, i.e., the lower estimate of pressure for garnet stability in metabasic rocks (Green et al., 2016; Wei and Duan, 2019). Further work is needed to fully constrain the metamorphic history of the Dadeville Complex rocks and may provide important insights into the tectonic evolution of the southern Appalachians.

6.5. Origin of the Dadeville Complex

Prevailing tectonic models for the northern Appalachians (Hibbard et al., 2007; van Staal and Barr, 2012) suggest that subduction initiated with eastward dip (present-day reference) at ca. 500–490 Ma, followed by terrane accretion and subsequent subduction polarity reversal at ca. 480 Ma. These models can account for more complete ophiolite sequences in the northern Appalachians, including preservation of mantle tectonites, layered ultramafics, a gabbroic section, sheeted dikes, and a metamorphic sole. The geometry of this model—where the forearc section formed during subduction initiation and was primed for obduction onto a peri-Laurentian terrane along the subduction thrust of the eastward-dipping subduction zone—can account for such complete preservation in the northern Appalachians (Stern, 2004; Stern et al., 2012). In the northern Appalachians, obduction (overthrusting) of the complexes also resulted in only greenschist-facies to lower-amphibolite-facies conditions, differing significantly from the higher *P-T* conditions typically recorded by mafic-ultramafic complexes of the southern Appalachians (Anderson and Moecher, 2009).

To explain the lesser abundance, inferior preservation, and higher metamorphic grade of the southern Appalachian mafic-ultramafic oceanic rocks, we propose a model wherein portions of forearc lithosphere were tectonically eroded, underthrusted, and/or carried to depth via subduction, to be exhumed during later tectonic events. According to this model, the divergent fates of forearc lithosphere from the northern and southern Appalachians can be reconciled by the polarity of the initiating subduction zone: The southern Appalachian mafic-ultramafic rocks record forearc lithosphere formed above a westward-dipping (rather than eastward-dipping) subduction zone in the Iapetus Ocean. This model (illustrated in Fig. 9) is consistent with previous interpretations of the Dadeville Complex having formed on the Laurentian (continental) side of the subduction trench, above a westward-dipping subduction zone (Barineau et al., 2015; Tull et al., 2014, 2018). The development of the similarly aged Wedowee-Emuckfaw-Dahlonega basin backarc in the overriding plate is also consistent with westward subduction of the Iapetan lithosphere under continental lithosphere of the Laurentian margin (Barineau et al., 2015, 2022; Tull et al., 2014, 2018).

7. CONCLUSIONS

(1) The Dadeville Complex represents a sequence of forearc basalts, boninites, and island-arc tholeiites.

(2) The up-stratigraphic-section evolution in geochemistry from forearc basalt to boninite is consistent with the forearc/protoarc volcanic rocks found in the Izu-Bonin-Mariana forearc and other suprasubduction zone ophiolites.

(3) A CA-ID-TIMS U-Pb zircon date of 467 ± 0.13 Ma (2σ) for the Dadeville Complex is interpreted to date subduction initiation (and forearc/protoarc spreading in the Iapetus Ocean).

(4) Granulite-facies conditions of >7 kbar and >760 °C are recorded by the Dadeville Complex rocks, suggesting deep underthrusting of the

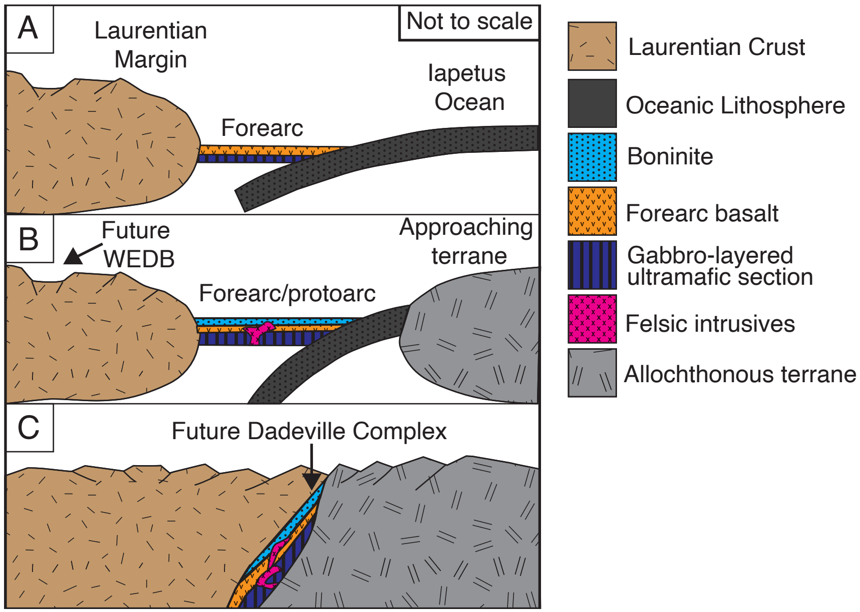

Figure 9. Tectonic model for formation of the Dadeville Complex. (A) Early to Middle Ordovician extension caused by slab foundering produces forearc lithosphere in response to seafloor spreading above the recently initiated subduction zone. (B) A second phase of magmatism—resulting from nascent flux melting of the depleted mantle lithosphere—produces boninite basalts. These overlie the forearc basalt and underlie the island-arc tholeiites, together comprising the volcanic portion of the subduction zone forearc lithosphere. (C) Forearc lithosphere is underthrust beneath the Laurentian margin, subjecting it to granulite-facies metamorphism. WEDB—Wedowee-Emuckfaw-Dalonega basin.

forearc/protoarc sequence (Dadeville Complex) during the subsequent convergence history.

(5) We propose that earliest subduction in the Alabama-Georgia sector of the Appalachians was westward-dipping (current coordinates) and developed proximal to the Laurentian margin.

ACKNOWLEDGMENTS

We thank Wentao Cao, Chong Ma, and James Tull for their thorough reviews, which improved the manuscript. Dana Brenner, Josh Garber, and Stanley Mertzman are thanked for their assistance with whole-rock laser ablation–inductively coupled plasma–mass spectrometry (LA-ICP-MS) and X-ray fluorescence (XRF) analysis. Mark Caddick is thanked for providing access to the Virginia Tech laboratory for additional major-element XRF analysis.

Funding for this project was provided by a National Science Foundation CAREER Grant (NSF-2042631), Johns Hopkins University (JHU) Catalyst Grant, Hopkins Extreme Materials Institute Seed Grant, JHU Department of Earth and Planetary Sciences Field Research Grant, Explorers Club Washington Group Exploration and Field Research Grant, Geologic Society of America Graduate Student Research Grant, and JHU Krieger School of Arts and Sciences J. Brien Key Fund Award.

We acknowledge the historical and continuing connection between Indigenous people and their native lands and specifically acknowledge that our research in the Dadeville Complex was performed on the stolen ancestral lands of the peoples of the Muscogee Nation (https://www.muscogeenation.com). We recognize their historical and ongoing resistance to settler occupation and offer this land acknowledgment to promote reflection and support of Indigenous movements for identity, freedom, and self-determination.

REFERENCES CITED

Adams, M.G., Stewart, K.G., Trupe, C.H., and Willard, R.A., 1995, Tectonic significance of high-pressure metamorphic rocks and dextral strike-slip faulting along the Taconic suture, *in* Hibbard, J.P., van Staal, C.R., and Cawood, P.A., eds., Current Perspectives in the Appalachian-Caledonian Orogen: Geological Association of Canada Special Paper 41, p. 21–42.

Anderson, E.D., and Moecher, D.P., 2009, Formation of high-pressure metabasites in the southern Appalachian Blue Ridge via Taconic continental subduction beneath the Laurentian margin: Tectonics, v. 28, TC5012, https://doi.org/10.1029/2008TC002319.

Andò, S., 2020, Gravimetric separation of heavy minerals in sediments and rocks: Minerals (Basel), v. 10, no. 3, p. 273, https://doi.org/10.3390/min10030273.

Arculus, R.J., Ishizuka, O., Bogus, K.A., et al., 2015, A record of spontaneous subduction initiation in the Izu-Bonin-Mariana arc: Nature Geoscience, v. 8, p. 728–733, https://doi.org/10.1038/ngeo2515.

Barineau, C., Tull, J.F., and Holm-Denoma, C.S., 2015, A Laurentian margin back-arc: The Ordovician Wedowee-Emuckfaw-Dahlonega basin, *in* Holmes, A.E., ed., Diverse excursions in the Southeast: Paleozoic to Present: Geological Society of America Field Guide 39, p. 21–78, https://doi.org/10.1130/2015.0039(02).

Barineau, C.I., Sagul, D.A., and Mueller, P.A., 2022, Ordovician–Silurian back-arc silicic magmatism in the southernmost Appalachians: Geological Society of America Bulletin, v. 134, no. 9–10, p. 2321–2334, https://doi.org/10.1130/B35948.1.

Barth, M.G., and Gluhak, T.M., 2009, Geochemistry and tectonic setting of mafic rocks from the Othris ophiolite, Greece: Contributions to Mineralogy and Petrology, v. 157, p. 23–40, https://doi.org/10.1007/s00410-008-0318-9.

Bédard, J.H., 1999, Petrogenesis of boninites from the Betts Cove ophiolite, Newfoundland, Canada: Identification of subducted source components: Journal of Petrology, v. 40, no. 12, p. 1853–1889, https://doi.org/10.1093/petroj/40.12.1853.

Bird, J., and Dewey, J., 1970, Lithosphere plate–continental margin tectonics and the evolution of the Appalachian orogen: Geological Society of America Bulletin, v. 81, p. 1031–1060, https://doi.org/10.1130/0016-7606(1970)81[1031:LPMTAT]2.0.CO;2.

Bird, J.M., Dewey, J.F., and Kidd, W.S.F., 1971, Proto-Atlantic oceanic crust and mantle: Appalachian/Caledonian ophiolites: Nature–Physical Science (London), v. 231, p. 28–31, https://doi.org/10.1038/physci231028a0.

Black, L.P., Kamo, S.L., Allen, C.M., Davis, D.W., Aleinikoff, J.N., Valley, J.W., Mundil, R., Campbell, I.H., Korsch, R.J., Williams, I.S., and Foudoulis, C., 2004, Improved $^{206}Pb/^{238}U$ microprobe geochronology by the monitoring of a trace-element-related matrix effect; SHRIMP, ID-TIMS, ELA-ICP-MS and oxygen isotope documentation for a series of zircon standards: Chemical Geology, v. 205, p. 115–140, https://doi.org/10.1016/j.chemgeo.2004.01.003.

Bream, B.R., 2003, Tectonic Implications of Para- and Orthogneiss Geochronology and Geochemistry from the Southern Appalachian Crystalline Core [Ph.D. thesis]: Knoxville, Tennessee, University of Tennessee, 310 p.

Brey, G.P., and Köhler, T., 1990, Geothermobarometry in four-phase lherzolites II. New thermobarometers, and practical assessment of existing thermobarometers: Journal of Petrology, v. 31, p. 1353–1378, https://doi.org/10.1093/petrology/31.6.1353.

Coler, D.G., Wortman, G.L., Samson, S.D., Hibbard, J.P., and Stern, R., 2000, U-Pb geochronologic, Nd isotopic, and

geochemical evidence for the correlation of the Chopawamsic and Milton terranes, Piedmont zone, southern Appalachian orogen: The Journal of Geology, v. 108, no. 4, p. 363–380, https://doi.org/10.1086/314411.
Crowley, J.L., Schoene, B., and Bowring, S.A., 2007, U-Pb dating of zircon in the Bishop Tuff at the millennial scale: Geology, v. 35, no. 12, p. 1123–1126, https://doi.org/10.1130/G24017A.1.
Crowley, W.P., 1976, The Geology of the Crystalline Rocks near Baltimore and its Bearing on the Evolution of the Eastern Maryland Piedmont: Maryland Geologic Survey Report of Investigations 27, 40 p., http://www.mgs.md.gov/publications/report_pages/RI_27.html.
Davis, B.L., 2021, Tectonostratigraphy, Geochemistry, and Geochronology of the Dadeville Complex of Alabama and Georgia: The Southern Appalachians Link to the Taconic Orogeny and Associated Suprasubduction System [Ph.D. thesis]: Tallahassee, Florida, Florida State University, 244 p.
De Souza, S., Tremblay, A., Daoust, C., and Gauthier, M., 2008, Stratigraphy and geochemistry of the Lac-Brompton ophiolite, Canada: Evidence for extensive forearc magmatism and mantle exhumation in the Southern Quebec ophiolite belt: Canadian Journal of Earth Sciences, v. 45, no. 9, p. 999–1014, https://doi.org/10.1139/E08-044.
Dilek, Y., and Furnes, H., 2011, Ophiolite genesis and global tectonics: Geochemical and tectonic fingerprinting of ancient oceanic lithosphere: Geological Society of America Bulletin, v. 123, p. 387–411, https://doi.org/10.1130/B30446.1.
Dilek, Y., and Thy, P., 2009, Island arc tholeiite to boninitic melt evolution of the Cretaceous Kizildag (Turkey) ophiolite: Model for multi-stage early arc-forearc magmatism in Tethyan subduction factories: Lithos, v. 113, no. 1–2, p. 68–87, https://doi.org/10.1016/j.lithos.2009.05.044.
Drake, A.A., Jr., and Morgan, B.A., 1981, The Piney Branch Complex—A metamorphosed fragment of the central Appalachian ophiolite in northern Virginia: American Journal of Science, v. 281, p. 484–508, https://doi.org/10.2475/ajs.281.4.484.
Drummond, M.S., Neilson, M.J., Allison, D.T., and Tull, J.F., 1997, Igneous petrogenesis and tectonic setting of granitic rocks from the eastern Blue Ridge and Inner Piedmont, Alabama Appalachians, *in* Sinha, A.K., Whalen, J.B., and Hogan, J.P., eds., The Nature of Magmatism in the Appalachian Orogen: Geological Society of America Memoir 191, p. 147–164, https://doi.org/10.1130/0-8137-1191-6.147.
Farris, D., Tull, J., Mueller, P., and Davis, B., 2017, Is the Dadeville Complex part of the "missing" southern Appalachian Taconic arc?, *in* Barineau, C.I., and Tull, J.F., eds., A Taconic Backarc and Arc Terrane in the Southern Appalachians: Correlating Geologic Units of the Blue Ridge and Western Inner Piedmont of Georgia and Alabama: Georgia Geological Society Guidebook 51, p. 41–56.
Furnes, H., Pedersen, R.B., and Stillman, C.J., 1988, The Leka ophiolite complex, central Norwegian Caledonides: Field characteristics and geotectonic significance: Journal of the Geological Society, v. 145, p. 401–412, https://doi.org/10.1144/gsjgs.145.3.0401.
Gerstenberger, H., and Haase, G., 1997, A highly effective emitter substance for mass spectrometric Pb isotope ratio determinations: Chemical Geology, v. 136, p. 309–312, https://doi.org/10.1016/S0009-2541(96)00033-2.
Green, E.C.R., White, R.W., Diener, J.F.A., Powell, R., Holland, T.J.B., and Palin, R.M., 2016, Activity-composition relations for the calculation of partial melting equilibria in metabasic rocks: Journal of Metamorphic Geology, v. 34, p. 845–869, https://doi.org/10.1111/jmg.12211.
Guice, G., McDonald, I., Hughes, H., Schlatter, D., Goodenough, K., MacDonald, J., and Faithfull, J., 2018, Assessing the validity of negative high field strength-element anomalies as a proxy for Archean subduction: Evidence from the Ben Strome Complex, NW Scotland: Geosciences, v. 8, p. 338, https://doi.org/10.3390/geosciences8090338.
Guice, G.L., McDonald, I., Hughes, H.S.R., and Anhaeusser, C.R., 2019, An evaluation of element mobility in the Modderfontein ultramafic complex, Johannesburg: Origin as an Archaean ophiolite fragment or greenstone belt remnant?: Lithos, v. 332–333, p. 99–119, https://doi.org/10.1016/j.lithos.2019.02.013.
Guice, G.L., Ackerson, M.R., Holder, R.M., George, F.R., Browning-Hanson, J.F., Burgess, J.L., Foustoukos, D.I., Becker, N.A., Nelson, W.R., and Viete, D.R., 2021, Suprasubduction zone ophiolite fragments in the central Appalachian orogen: Evidence for mantle and Moho in the Baltimore Mafic Complex (Maryland, USA): Geosphere, v. 17, p. 561–581, https://doi.org/10.1130/GES02289.1.
Hibbard, J., 2000, Docking Carolina: Mid-Paleozoic accretion in the southern Appalachians: Geology, v. 28, p. 127–130, https://doi.org/10.1130/0091-7613(2000)28<127:DCMAIT>2.0.CO;2.
Hibbard, J.P., van Staal, C.R., and Rankin, D.W., 2007, A comparative analysis of pre-Silurian crustal building blocks of the northern and the southern Appalachian orogen: American Journal of Science, v. 307, p. 23–45, https://doi.org/10.2475/01.2007.02.
Hiess, J., Condon, D.J., McLean, N., and Noble, S.R., 2012, $^{238}U/^{235}U$ systematics in terrestrial uranium-bearing minerals: Science, v. 335, p. 1610–1614, https://doi.org/10.1126/science.1215507.
Holm-Denoma, C.S., and Das, R., 2010, Bimodal volcanism as evidence for Paleozoic extensional accretionary tectonism in the southern Appalachians: Geological Society of America Bulletin, v. 122, p. 1220–1234, https://doi.org/10.1130/B30051.1.
Horstwood, M.S.A., Košler, J., Gehrels, G., Jackson, S.E., McLean, N.M., Paton, C., Pearson, N.J., Sircombe, K., Sylvester, P., Vermeesch, P., Bowring, J.F., Condon, D.J., and Schoene, B., 2016, Community-derived standards for LA-ICP-MS U-(Th-)Pb geochronology—Uncertainty propagation, age interpretation and data reporting: Geostandards and Geoanalytical Research, v. 40, p. 311–332, https://doi.org/10.1111/j.1751-908X.2016.00379.x.
Horton, J.W., Jr., Drake, A.A., Jr., and Rankin, D.W., 1989, Tectonostratigraphic terranes and their Paleozoic boundaries in the central and southern Appalachians, *in* Dallmeyer, R.D., ed., Terranes in the Circum-Atlantic Paleozoic Orogens: Geological Society of America Special Paper 230, p. 213–245, https://doi.org/10.1130/SPE230-p213.
Horton, J.W., Jr., Aleinikoff, J.N., Drake, A.A., Jr., and Fanning, C.M., 1998, Significance of Middle to Late Ordovician volcanic-arc rocks in the central Appalachian Piedmont, Maryland and Virginia: Geological Society of America Abstracts with Programs, v. 30, no. 7, p. 125.
Irvine, T.N., and Baragar, W.R.A., 1971, A guide to the chemical classification of the common volcanic rocks: Canadian Journal of Earth Sciences, v. 8.5, p. 523–548, https://doi.org/10.1139/e71-055.
Ishikawa, T., Nagaishi, K., and Umino, S., 2002, Boninitic volcanism in the Oman ophiolite: Implications for thermal condition during transition from spreading ridge to arc: Geology, v. 30, no. 10, p. 899–902, https://doi.org/10.1130/0091-7613(2002)030<0899:BVITOO>2.0.CO;2.
Ishizuka, O., Tani, K., Reagan, M.K., Kanayama, K., Umino, S., Harigane, Y., Sakamoto, I., Miyajima, Y., Yuasa, M., and Dunkley, D.J., 2011, The timescales of subduction initiation and subsequent evolution of an oceanic island arc: Earth and Planetary Science Letters, v. 306, p. 229–240, https://doi.org/10.1016/j.epsl.2011.04.006.
Jaffey, A.H., Flynn, K.F., Glendenin, L.E., Bentley, W.C., and Essling, A.M., 1971, Precision measurement of half-lives and specific activities of ^{235}U and ^{238}U: Physical Review C: Nuclear Physics, v. 4, p. 1889–1906, https://doi.org/10.1103/PhysRevC.4.1889.
Jochum, K.P., Nohl, U., Herwig, K., Lammel, E., Stoll, B., and Hofmann, A.W., 2005, GeoReM: A new geochemical database for reference materials and isotopic standards: Geostandards and Geoanalytical Research, v. 29, p. 333–338, https://doi.org/10.1111/j.1751-908X.2005.tb00904.x.
Krogh, T.E., 1973, A low-contamination method for hydrothermal decomposition of zircon and extraction of U and Pb for isotopic age determinations: Geochimica et Cosmochimica Acta, v. 37, p. 485–494, https://doi.org/10.1016/0016-7037(73)90213-5.
Lawton, D.E., Moye, F.J., Murray, J.B., O'Connor, B.J., Penley, H.M., Sandrock, G.S., Marsalis, W.E., Friddell, M.S., Hetrick, J.H., Huddlestun, P.F., Hunter, R.E., Mann, W.R., Martin, B.F., Pickering, S.M., Schneeberger, F.J., and Wilson, J.D., 1976, Geologic Map of Georgia: Atlanta, Georgia, Georgia Geological Survey, scale 1:500,000.
Leng, W., Gurnis, M., and Asimow, P., 2012, From basalts to boninites: The geodynamics of volcanic expression during induced subduction initiation: Lithosphere, v. 4, p. 511–523, https://doi.org/10.1130/L215.1.
Li, H., Arculus, R.J., Ishizuka, O., Hickey-Vargas, R., Yogodzinski, G.M., McCarthy, A., Kusano, Y., Brandl, P.A., Savov, I.P., Teplet, F.J., III, and Sun, W., 2021, Basalt derived from highly refractory mantle sources during early Izu-Bonin-Mariana arc development: Nature Communications, v. 12, https://doi.org/10.1038/s41467-021-21980-0.
Ludwig, K.R., 2003, User's Manual for Isoplot 3.00: Berkeley, California, Berkeley Geochronology Center, 70 p.
Ma, C., Vandervoort, D.S., Steltenpohl, M.G., and Schwartz, J.J., 2019, Formation and orogen-parallel transport of the Dadeville Complex, Alabama, USA: Implications for the Taconian orogeny in the southern Appalachians: American Journal of Science, v. 319, p. 582–630, https://doi.org/10.2475/07.2019.03.
Mattinson, J.M., 2005, Zircon U-Pb chemical abrasion ("CA-TIMS") method: Combined annealing and multi-step partial dissolution analysis for improved precision and accuracy of zircon ages: Chemical Geology, v. 220, p. 47–66, https://doi.org/10.1016/j.chemgeo.2005.03.011.
McClellan, E.A., Steltenpohl, M.G., Thomas, C., and Miller, C.F., 2007, Isotopic age constraints and metamorphic history of the Talladega belt: New evidence for timing of arc magmatism and terrane emplacement along the southern

Laurentian margin: The Journal of Geology, v. 115, p. 541–561, https://doi.org/10.1086/519777.

McElhaney, M.S., and McSween, H.Y., Jr., 1983, Petrology of the Chunky Gal Mountain mafic-ultramafic complex, North Carolina: Geological Society of America Bulletin, v. 94, p. 855–874, https://doi.org/10.1130/0016-7606(1983)94<855:POTCGM>2.0.CO;2.

Merschat, A.J., Hatcher, R.D., Ryan Thigpen, J., and McClellan, E.A., 2018, Blue Ridge–Inner Piedmont geotraverse from the Great Smoky fault to the Inner Piedmont: Upper crust to upper-lower crust, terranes, large faults, and sutures, *in* Engel, A.S., and Hatcher, R.D., Jr., eds., Geology at Every Scale: Field Excursions for the 2018 GSA Southeastern Section Meeting in Knoxville, Tennessee: Geological Society of America Field Guide 50, p. 141–209, https://doi.org/10.1130/2018.0050(09).

Miller, B.V., Fetter, A.H., and Stewart, K.G., 2006, Plutonism in three orogenic pulses, Eastern Blue Ridge Province, southern Appalachians: Geological Society of America Bulletin, v. 118, p. 171–184, https://doi.org/10.1130/B25580.1.

Misra, K.C., and Conte, J.A., 1991, Amphibolites of the Ashe and Alligator Back formations, North Carolina: Samples of late Proterozoic–early Paleozoic oceanic crust: Geological Society of America Bulletin, v. 103, p. 737–750, https://doi.org/10.1130/0016-7606(1991)103<0737:AOTAAA>2.3.CO;2.

Mittwede, S.K., 1989, The Hammett Grove Meta-igneous Suite: A possible ophiolite in the northwestern South Carolina Piedmont, *in* Mittwede, S.K., and Stoddard, E.F., eds., Ultramafic Rocks of the Appalachian Piedmont: Geological Society of America Special Paper 231, p. 45–62, https://doi.org/10.1130/SPE231-p45.

Muller, P.D., Candela, P.A., and Wylie, A.G., 1989, Liberty Complex: Polygenetic mélange in the central Maryland Piedmont, *in* Horton, J.W., Jr., and Rast, N., eds., Mélanges and Olistostromes of the U.S. Appalachians: Geological Society of America Special Paper 228, p. 113–134, https://doi.org/10.1130/SPE228-p113.

Neilson, M.J., 1983, Structure and stratigraphy of the Dadeville Group within the Tallassee synform, Tallapoosa County, Alabama: Geological Society of America Abstracts with Programs, v. 15, no. 2, p. 110.

Neilson, M.J., and Bittner, E.I., 1990, General lithology and petrology of the Dadeville Complex, in Steltenpohl, M.G., Neilson, M.J., Bittner, E.I., Colberg, M.R., and Cook, R.B., eds., Geology of the Southern Inner Piedmont, Alabama and Southwest Georgia: Field Trip No. 7: Southeastern Section, Geological Society of America, 39th Annual Meeting Guidebook for Field Trips, Tuscaloosa, Alabama, p. 65–77.

Neilson, M.J., and Stow, S.H., 1986, Geology and geochemistry of the mafic and ultramafic intrusive rocks, Dadeville belt, Alabama: Geological Society of America Bulletin, v. 97, p. 296–304, https://doi.org/10.1130/0016-7606(1986)97<296:GAGOTM>2.0.CO;2.

Neilson, M.J., Seal, T.L., and Kish, S.A., 1997, Two high-silica gneisses from the Dadeville Complex of Alabama's Inner Piedmont: Southeastern Geology, v. 36, p. 123–132.

Olive, V., Hébert, R., and Loubet, M., 1997, Isotopic and trace element constraints on the genesis of a boninitic sequence in the Thetford Mines ophiolitic complex, Quebec, Canada: Canadian Journal of Earth Sciences, v. 34, p. 1258–1271, https://doi.org/10.1139/e17-100.

Oliver, G.J.H., and McAlpine, R.R., 1998, Occurrence of a sheeted dyke complex in the Ballantrae ophiolite, Scotland: Geological Magazine, v. 135, no. 4, p. 509–517, https://doi.org/10.1017/S0016756898001162.

Osborne, W.E., Szabo, E.W., Copeland, C.W., Jr., and Neathery, T.L., 1989, Geologic Map of Alabama: Tuscaloosa, Alabama, Geological Survey of Alabama, scale 1:500,000.

Paces, J.B., and Miller, J.D., Jr., 1993, Precise U-Pb ages of Duluth Complex and related mafic intrusions, northeastern Minnesota: Geochronological insights to physical, petrogenetic, paleomagnetic, and tectonomagmatic processes associated with the 1.1 Ga Midcontinent Rift system: Journal of Geophysical Research: Solid Earth, v. 98, p. 13,997–14,013, https://doi.org/10.1029/93JB01159.

Paton, C., Woodhead, J.D., Hellstrom, J.C., Hergt, J.M., Greig, A., and Maas, R., 2010, Improved laser ablation U-Pb zircon geochronology through robust downhole fractionation correction: Geochemistry, Geophysics, Geosystems, v. 11, no. 3, Q0AA06, https://doi.org/10.1029/2009GC002618.

Paton, C., Hellstrom, J., Paul, B., Woodhead, J., and Hergt, J., 2011, Iolite: free-ware for the visualisation and processing of mass spectrometric data: Journal of Analytical Atomic Spectrometry, v. 26, no. 12, p. 2508–2518, https://doi.org/10.1039/c1ja10172b.

Pearce, J.A., and Reagan, M.K., 2019, Identification, classification, and interpretation of boninites from Anthropocene to Eoarchean using Si-Mg-Ti systematics: Geosphere, v. 15, p. 1008–1037, https://doi.org/10.1130/GES01661.1.

Pearce, J.A., Reagan, M.K., Petronotis, K., et al., 2015, International Ocean Discovery Program Expedition 352 Preliminary Report: Izu-Bonin-Mariana Fore Arc: Testing Subduction Initiation and Ophiolite Models by Drilling the Outer Izu-Bonin-Mariana Fore Arc: College Station, Texas, International Ocean Discovery Program, 86 p., https://doi.org/10.14379/iodp.pr.352.2015.

Pedersen, R.B., and Furnes, H., 1991, Geology, magmatic affinity and geotectonic environment of some Caledonian ophiolites in Norway: Journal of Geodynamics, v. 13, p. 183–203, https://doi.org/10.1016/0264-3707(91)90038-G.

Pedersen, R.B., Furnes, H., and Dunning, G.R., 1988, Some Norwegian ophiolite complexes reconsidered, *in* Kristoffersen, Y., ed., Progress the Studies of the Lithosphere in Norway: Norges Geologiske Undersøkelse Special Publication 3, p. 80–85.

Peterson, V., and Ryan, J.G., 2009, Petrogenesis and structure of the Buck Creek mafic-ultramafic suite, southern Appalachians: Constraints on ophiolite evolution and emplacement in collisional orogens: Geological Society of America Bulletin, v. 121, p. 615–629, https://doi.org/10.1130/B26302.1.

Pollock, J.C., Hibbard, J.P., and van Staal, C.R., 2012, A paleogeographical review of the peri-Gondwanan realm of the Appalachian orogen: Canadian Journal of Earth Sciences, v. 49, p. 259–288, https://doi.org/10.1139/e11-049.

Portnyagin, M.V., Danyushevsky, L.V., and Kamenetsky, V.S., 1997, Coexistence of two distinct mantle sources during formation of ophiolites: A case study of primitive pillow-lavas from the lowest part of the volcanic section of the Troodos Ophiolite, Cyprus: Contributions to Mineralogy and Petrology, v. 128, p. 287–301, https://doi.org/10.1007/s004100050309.

Rankin, D.W., 1994, Continental margin of the eastern United States: Past and present, *in* Speed, R.C., ed., Phanerozoic Evolution of North American Continent-Ocean Transitions: Boulder, Colorado, Geological Society of America, Decade of North American Geology Continent-Ocean Transect Series Summary Volume, p. 129–218, https://doi.org/10.1130/DNAG-COT-PEN.129.

Raymond, L., Swanson, S., Love, A., and Allan, J., 2003, Cr-spinel compositions, metadunite petrology, and the petrotectonic history of Blue Ridge ophiolites, southern Appalachian orogen, USA, *in* Dilek, Y., and Robinson, P.T., eds., Ophiolites in Earth History: Geological Society, London, Special Publication 18, p. 218–253, https://doi.org/10.1144/GSL.SP.2003.218.01.14.

Raymond, L.A., Merschat, A., and Vance, R.K., 2016, Metaultramafic schists and dismembered ophiolites of the Ashe metamorphic suite of northwestern North Carolina, USA: International Geology Review, v. 58, p. 874–912, https://doi.org/10.1080/00206814.2015.1129515.

Reagan, M.K., Ishizuka, O., Stern, R.J., Kelley, K.A., Ohara, Y., Blichert-Toft, J., Bloomer, S.H., Cash, J., Freyer, P., Hanan, B.B., Hickey-Vargas, R., Ishii, T., Kimura, J., Peate, D.W., Rowe, M.C., and Woods, M., 2010, Fore-arc basalts and subduction initiation in the Izu-Bonin-Mariana system: Geochemistry Geophysics Geosystems, v. 11, p. 1–17, https://doi.org/10.1029/2009GC002871.

Reagan, M.K., Pearce, J.A., Petronotis, K., Almeev, R., Avery, A.A., Carvallo, C., Chapman, T., Christeson, G.L., Ferré, E.C., Godard, M., Heaton, D.E., Kirchenbaur, M., Kurz, W., Kutterolf, S., Li, H.Y., Li, Y., Michibayashi, K., Morgan, S., Nelson, W.R., Prytulak, J., Python, M., Robertson, A.H.F., Ryan, J.G., Sager, W.W., Sakuyama, T., Shervais, J.W., Shimizu, K., and Whattam, S.A., 2015, Proceedings of the International Ocean Discovery Program: Expedition 352 Summary: College Station, Texas, International Ocean Discovery Program, 32 p., https://doi.org/10.14379/iodp.proc.352.101.2015.

Reagan, M.K., Heaton, D.E., Schmitz, M.D., Pearce, J.A., Shervais, J.W., and Koppers, A.A.P., 2019, Forearc ages reveal extensive short-lived and rapid seafloor spreading following subduction initiation: Earth and Planetary Science Letters, v. 506, p. 520–529, https://doi.org/10.1016/j.epsl.2018.11.020.

Rioux, M., Garber, J.M., Searle, M., Kelemen, P., Miyashita, S., Adachi, Y., and Bowring, S., 2021, High-precision U-Pb zircon dating of late magmatism in the Samail Ophiolite: A record of subduction initiation: Journal of Geophysical Research: Solid Earth, v. 126, p. 1–26, https://doi.org/10.1029/2020JB020758.

Rodgers, J., 1971, The Taconic orogeny: Geological Society of America Bulletin, v. 82, no. 5, p. 1141–1177, https://doi.org/10.1130/0016-7606(1971)82[1141:TTO]2.0.CO;2.

Schaltegger, U., Schmitt, A.K., and Horstwood, M.S.A., 2015, U-Th-Pb zircon geochronology by ID-TIMS, SIMS and laser ablation ICP-MS: Recipes, interpretations, and opportunities: Chemical Geology, v. 402, p. 89–110, https://doi.org/10.1016/j.chemgeo.2015.02.028.

Schmitz, M.D., and Schoene, B., 2007, Derivation of isotope ratios, errors, and error correlations for U-Pb geochronology using ^{205}Pb-^{235}U-(^{233}U)-spiked isotope dilution thermal ionization mass spectrometric data: Geochemistry Geophysics Geosystems, v. 8, Q08006, https://doi.org/10.1029/2006GC001492.

Schoene, B., Crowley, J.L., Condon, D.J., Schmitz, M.D., and Bowring, S.A., 2006, Reassessing the uranium decay constants for geochronology using ID-TIMS U-Pb data: Geochimica et Cosmochimica Acta, v. 70, no. 2, p. 426–445, https://doi.org/10.1016/j.gca.2005.09.007.

Seal, T.L., and Kish, S.A., 1990, The geology of the Dadeville Complex of the western Georgia and eastern Alabama Inner Piedmont: Initial petrographic, geochemical, and geochronological results, *in* Steltenpohl, M.G., Neilson, M.J., Bittner, E.I., Colberg, M.R., and Cook, R.B., eds., Geology of the Southern Inner Piedmont, Alabama and Southwest Georgia, Field Trip No. 7: Southeastern Section, Geological Society of America, Tuscaloosa, Alabama, 39th Annual Meeting Guidebook for Field Trips, p. 65–77.

Settles, D.J., 2002, Defining the Hayesville–Soque River and Allatoona Faults and an Ordovician Arc Assemblage Within the Central Blue Ridge Northwest of Dahlonega, Georgia [M.S. thesis]: Knoxville, Tennessee, University of Tennessee, 148 p.

Shervais, J.W., Kimbrough, D.L., Renne, P., Hanan, B.B., Murchey, B., Snow, C.A., Zoglman Schuman, M.M., and Beaman, J., 2004, Multi-stage origin of the Coast Range ophiolite, California: Implications for the life cycle of supra-subduction zone ophiolites: International Geology Review, v. 46, no. 4, p. 289–315, https://doi.org/10.2747/0020-6814.46.4.289.

Shervais, J.W., et al., 2019, Magmatic response to subduction initiation: Part 1. Fore-arc basalts of the Izu-Bonin arc from IODP Expedition 352: Geochemistry, Geophysics, Geosystems, v. 20, p. 314–338, https://doi.org/10.1029/2018GC007731.

Shervais, J.W., et al., 2021, Magmatic response to subduction initiation: Part II. Boninites and related rocks of the Izu-Bonin arc from IODP Expedition 352: Geochemistry, Geophysics, Geosystems, v. 22, p. 1–34, https://doi.org/10.1029/2020GC009093.

Sláma, J., Košler, J., Condon, D.J., Crowley, J.L., Gerdes, A., Hanchar, J.M., Horstwood, M.S.A., Morris, G.A., Nasdala, L., Norberg, N., Schaltegger, U., Schoene, B., Tubrett, M.N., and Whitehouse, M.J., 2008, Plešovice zircon—A new natural reference material for U-Pb and Hf isotopic microanalysis: Chemical Geology, v. 249, p. 1–35, https://doi.org/10.1016/j.chemgeo.2007.11.005.

Spell, T.L., and Norrell, G.T., 1990, The Ropes Creek assemblage: Petrology, geochemistry, and tectonic setting of an ophiolitic thrust sheet in the southern Appalachians: American Journal of Science, v. 290, no. 7, p. 811–842, https://doi.org/10.2475/ajs.290.7.811.

Steltenpohl, M.G., Horton, J.W., Hatcher, R.D., Zietz, I., Daniels, D.L., and Higgins, M.W., 2013, Upper crustal structure of Alabama from regional magnetic and gravity data: Using geology to interpret geophysics, and vice versa: Geosphere, v. 9, no. 4, p. 1044–1064, https://doi.org/10.1130/GES00703.1.

Sterling, J.W., 2006, Geology of the Southernmost Exposures of the Brevard Zone in the Red Hill Quadrangle, Alabama [M.S. thesis]: Auburn, Alabama, Auburn University, 133 p.

Stern, R.J., 2004, Subduction initiation: spontaneous and induced: Earth and Planetary Science Letters, v. 226, p. 275–292, https://doi.org/10.1016/j.epsl.2004.08.007.

Stern, R.J., Reagan, M., Ishizuka, O., Ohara, Y., and Whattam, S., 2012, To understand subduction initiation, study forearc crust: To understand forearc crust, study ophiolites: Lithosphere, v. 4, no. 6, p. 469–483, https://doi.org/10.1130/L183.1.

Stevens, A.J., 2018, Relationship between the Dadeville Complex and Opelika Group, Appalachian Inner Piedmont of Alabama and Georgia [M.S. thesis]: Tallahassee, Florida, Florida State University, 74 p.

Stewart, K.G., Adams, M.G., and Trupe, C.H., 1997, Paleozoic structural evolution of the Blue Ridge thrust complex, western North Carolina, *in* Stewart, K.G., Adams, M.G., and Trupe, C.H., eds., Paleozoic Structure, Metamorphism, and Tectonics of the Blue Ridge of Western North Carolina, 1997 Field Trip Guidebook: Chapel Hill, North Carolina, Carolina Geological Society, p. 21–31.

St-Onge, M.R., and Ijewliw, O.J., 1996, Mineral corona formation during high-*P* retrogression of granulitic rocks, Ungava orogen, Canada: Journal of Petrology, v. 37, no. 3, p. 553–582, https://doi.org/10.1093/petrology/37.3.553.

Stow, S.H., Neilson, M.J., and Neathery, T.L., 1984, Petrography, geochemistry, and tectonic significance of the amphibolites of the Alabama Piedmont: American Journal of Science, v. 284, no. 4–5, p. 414–436, https://doi.org/10.2475/ajs.284.4-5.414.

Sun, S.S., and McDonough, W.F., 1989, Chemical and isotopic systematics of oceanic basalts: Implications for mantle composition and processes, *in* Saunders, A.D., and Norry, M.J., eds., Magmatism in the Ocean Basins: Geological Society, London, Special Publication 42, p. 313–345, https://doi.org/10.1144/GSL.SP.1989.042.01.19.

Tenthorey, E.A., Ryan, J.G., and Snow, E.A., 1996, Petrogenesis of sapphirine-bearing metatroctolites from the Buck Creek ultramafic body, southern Appalachians: Journal of Metamorphic Geology, v. 14, p. 103–114, https://doi.org/10.1046/j.1525-1314.1996.05793.x.

Thomas, C.W., 2001, Origins of Mafic-Ultramafic Complexes of the Eastern Blue Ridge Province, Southern Appalachians: Geochronological and Geochemical Constraints [M.S. thesis]: Nashville, Tennessee, Vanderbilt University, 154 p.

Tull, J.F., Barineau, C.I., Mueller, P.A., and Wooden, J.L., 2007, Volcanic arc emplacement onto the southernmost Appalachian Laurentian shelf: Characteristics and constraints: Geological Society of America Bulletin, v. 119, p. 261–274, https://doi.org/10.1130/B25998.1.

Tull, J.F., Holm-Denoma, C.S., and Barineau, C.I., 2014, Early to Middle Ordovician back-arc basin in the southern Appalachian Blue Ridge: Characteristics, extent, and tectonic significance: Geological Society of America Bulletin, v. 126, p. 990–1015, https://doi.org/10.1130/B30967.1.

Tull, J.F., Mueller, P.A., Farris, D.W., and Davis, B.L., 2018, Taconic suprasubduction zone magmatism in southern Laurentia: Evidence from the Dadeville Complex: Geological Society of America Bulletin, v. 130, no. 7–8, p. 1339–1354, https://doi.org/10.1130/B31885.1.

Vandervoort, D.S., 2016, Geology of the Wadley South Quadrangle and Geochronology of the Dadeville Complex, Southernmost Appalachians of East Alabama [M.S. thesis]: Auburn, Alabama, Auburn University, 127 p.

van Staal, C.R., and Barr, S.M., 2012, Lithospheric architecture and tectonic evolution of the Canadian Appalachians and associated Atlantic margin, *in* Percival, J.A., Cook, F.A., and Clowes, R.M., eds., Tectonic Styles in Canada: The LITHOPROBE Perspective: Geological Association of Canada Special Paper 49, p. 41–95.

Vermeesch, P., 2018, IsoplotR: A free and open toolbox for geochronology: Geoscience Frontiers, v. 9, no. 5, p. 1479–1493, https://doi.org/10.1016/j.gsf.2018.04.001.

Waldron, J.W.F., Murphy, J.B., Melchin, M.J., and Davis, G., 1996, Silurian tectonics of western Avalonia: Strain-corrected subsidence history of the Arisaig Group, Nova Scotia: The Journal of Geology, v. 104, no. 6, p. 677–694, https://doi.org/10.1086/629862.

Wei, C.J., and Duan, Z.Z., 2019, Phase relations in metabasic rocks: Constraints from the results of experiments, phase modelling and ACF analysis, *in* Zhang, L., Zhang, Z., Schertl, H.-P., and Wei, C.J., eds., UP-UHP Metamorphism and Tectonic Evolution of Orogenic Belts: Geological Society, London, Special Publication 474, p. 25–45, https://doi.org/10.1144/SP474.10.

Whattam, S.A., and Stern, R.J., 2011, The 'subduction initiation rule': A key for linking ophiolites, intra-oceanic forearcs, and subduction initiation: Contributions to Mineralogy and Petrology, v. 162, p. 1031–1045, https://doi.org/10.1007/s00410-011-0638-z.

Wiedenbeck, M., Allé, P., Corfu, F., Griffin, W.L., Meier, M., Oberli, F., Von Quadt, A., Roddick, J.C., and Spiegel, W., 1995, Three natural zircon standards for U-Th-Pb, Lu-Hf, trace element and REE analyses: Geostandards Newsletter, v. 19, p. 1–23, https://doi.org/10.1111/j.1751-908X.1995.tb00147.x.

Williams, H., and Hatcher, R.D., Jr., 1983, Appalachian suspect terranes, *in* Hatcher, R.D., Jr., Williams, H., and Zietz, I., eds., Contributions to the Tectonics and Geophysics of Mountain Chains: Geological Society of America Memoir 158, p. 33–53, https://doi.org/10.1130/MEM158-p33.

Yuan, C., Sun, M., Zhou, M.-F., Xiao, W., and Zhou, H., 2005, Geochemistry and petrogenesis of the Yishak volcanic sequence, Kudi ophiolite, West Kunlun (NW China): Implications for the magmatic evolution in a subduction zone environment: Contributions to Mineralogy and Petrology, v. 150, p. 195–211, https://doi.org/10.1007/s00410-005-0012-0.